Materials Today Communications 27 (2021) 102275

Contents lists available at ScienceDirect

Materials Today Communications

journal homepage: www.elsevier.com/locate/mtcomm

A review on electrodeposited layered double hydroxides for energy and environmental applications

R.C. Rohit [a], Ajay D. Jagadale [a,*], Surendra K. Shinde [b], D.-Y. Kim [b]

[a] Center for Energy Storage and Conversion, School of Electrical and Electronics Engineering, SASTRA Deemed University, Thanjavur, 613401, Tamilnadu, India
[b] Department of Biological and Environmental Science, College of Life Science and Biotechnology, Dongguk University, 32 Dongguk-ro, Biomedical Campus, Ilsandong-gu, Siksa-dong, 10326, Goyang-si, Gyeonggi-do, South Korea

ARTICLE INFO

Keywords:
Electrodeposition
Layered double hydroxide (LDH)
Supercapacitors
Electrocatalyst
Sensors

ABSTRACT

The great demand for efficient and low-cost materials for energy and environmental applications has been inspiring researchers to develop novel and advanced materials. Recently, layered double hydroxides (LDHs) are found to be admirable materials for various applications owing to their tunable elemental composition and diverse nanostructures. The preparation of binder-free LDHs thin-film electrodes has attracted great attention in the field of supercapacitors, electrocatalysts and sensors. The electrodeposition method exhibits the capability of fabricating binder-free, uniform and well-oriented thin films with tunable elemental composition. In the present review, we provide a detailed electrodeposition mechanism behind the formation of LDHs with nucleation and growth processes. Also, we summarize the literature on electrodeposited LDHs based electrode materials for energy and environmental applications. In energy storage applications, a loading amount of active materials on the substrate is crucial to improve the areal and volumetric capacities. Therefore, the utilization of low-cost and scalable scaffold materials such as carbon nanofibers, graphene foam, etc. is highly recommended.

1. Introduction

Layered double hydroxides (LDHs), often called hydrotalcite-like systems or anionic clays have attracted great attention owing to their tunable chemical and metal-anion compositions. The general formula for LDHs can be written as $[M^{II}_{1-x}M^{III}_{x}(OH)_2]^{x+}[A^{n-}_{x/n}\cdot yH_2O]^{x-}$ (where M^{II} and M^{III} represent the divalent and trivalent metal cations, A^{n-} represents n-valent anions). Depending upon the nature of cations and M^{II}/M^{III} molar ratios, LDHs can be prepared with a wide range of layered structures [1]. The tunability of the molar ratio of metal cations and the nature of interlaying compensating anions lead to the formation of different nanoarchitectures with versatile physical and chemical properties, extending their applicability in diverse fields [2]. LDHs have been reported for different energy and environmental applications such as electrochemical energy storage, electrocatalyst, sensors, etc. These applications demand well-oriented, uniform and high conducting thin films [3,4]. Previously, LDHs have been prepared by different chemical methods such as co-precipitation [5], hydrothermal [6], sol-gel [7] and urea hydrolysis [8], either in thin film or powder form. These chemical methods are time-consuming and complex. Also, the powdered materials need to be combined with binders and conducting additives to be applied for many energy and environment-related applications, imposing additional inactive mass to the electrode [9]. In order to overcome these disadvantages, a binder-free LDHs can be prepared using electrodeposition method. The electrodeposition is rapid, facile, and scalable method which deposits well oriented and high quality thin film materials on the conducting support with enhanced conductivity and electrochemically active sites [10]. Recently, variety of different LDHs thin films have been prepared using electrodeposition method. Fig. 1 shows the number of publications and number of citations received by the research papers published in the field of electrodeposited LDHs, indicating the influence of the field.

Recently, some review articles have been published in the field of LDHs [1,11–13]. However, they mainly focus on general synthesis methods and their different applications. To the best of our knowledge, there is no review article published that emphasizes the detailed electrodeposition mechanism behind the formation of LDHs and review of electrodeposited LDHs for energy and environmental applications. It is important to understand the detailed electrodeposition mechanism in preparing LDHs for a variety of applications to fabricate efficient materials by overcoming present difficulties. Therefore, in this review, we have discussed the fundamentals of electrodeposition methods with

* Corresponding author.
E-mail address: jagadaleajay99@gmail.com (A.D. Jagadale).

https://doi.org/10.1016/j.mtcomm.2021.102275
Received 18 January 2021; Received in revised form 11 March 2021; Accepted 22 March 2021
Available online 23 March 2021

nucleation and growth processes involved in the formation of LDHs. Moreover, we summarized the literature of electrodeposited LDHs based electrode materials with their performances in different energy and environmental applications. Finally, we discuss the current difficulties and future research prospects in the field.

2. Electrodeposition mechanism

As compared to other conventional methods, the electrodeposition has attained great attention owing to its several advantages such as low cost, large scale deposition, and control over elemental composition as well as the morphology of the material [14]. Previously, the electrodeposition of LDHs has been performed using a standard three-electrode system with nitrate-containing electrolyte and their suitability for various applications has been analyzed [14–16]. The general mechanism for the LDH deposition can be explained by the following electrochemical reactions.

$$NO_3^- + H_2O + 2e^- \rightarrow NO_2^- + 2OH^- \quad (1)$$

$$M^{2+} + 2OH^- \rightarrow M(OH)_2 \quad (2)$$

The deposition is carried out in the nitrate ions containing electrolyte and under cathodic conditions, nitrate ions from the electrolyte reduce to form hydroxide ions as shown in the reaction (1). The produced hydroxide ions enhance the pH at the surface of the substrate which further precipitates the metal cations to form LDHs. In reaction (2), M^{X+} represents the metal cations that precipitate with hydroxide ion, forming the LDH coating on the surface of the substrate [17].

2.1. Nucleation and growth of electrodeposited LDHs

The nucleation and growth of electrodeposited material can be divided into two major processes such as (A) deposition and (B) electrocrystallization [18]. The nucleation and growth processes are clearly illustrated in Fig. 2 which consists of 6 steps. In the first step, solvated ions (i.e. nitrate and metal cations (M^{II} and M^{III})) are driven towards the electric double layer formed near the surface of the substrate because of the mass transport mechanism. As hydrated nitrate ions approach the surface of the substrate, they lose the sheath of solvated water ions and a charge transfer reaction takes place. The formation of nitrate ad-ions may greatly depend on the surface energy of the substrate. Once nitrate ion partially touches the surface of the substrate, it attaches to the active site of the substrate and becomes an ad-ion. Still, some amount of water molecules are attached with the nitrate ad-ion due to the charge. In the next step, the charge transfer reaction occurs and hydroxide ions are formed. Simultaneously, metal cations from the electrolyte precipitate with the condensed hydroxyl ions to form a metal hydroxide deposit. This results in the construction of the lattice arrangements and finally stable atomic clusters.

3. Applications of electrodeposited LDHs

The electrodeposited LDHs and their composites have been reported for various applications, such as supercapacitors, electrocatalysts, sensors, electrochromism, water purification, etc. Based on different applications, LDHs and their composites can be classified as shown in Fig. 3. The performance of electrodeposited LDHs based materials can be described as follows.

3.1. LDHs for supercapacitors

Due to the higher power density and compatibility to integrate with other energy storage devices, supercapacitors have been exposed to a variety of applications such as transport, aerospace, and consumer electronics [19]. Based on the charge storage mechanism, supercapacitors can be commonly classified as electrochemical double-layer capacitors (EDLCs) and pseudocapacitors. The carbonaceous materials predominantly store the charge by EDLC mechanism, whereas metal oxides (RuO_2, MnO_2, etc.) and conducting polymers (polyaniline, polypyrrole, etc.) store the charge by fast redox reactions at/near the electrode surface (pseudocapacitance) [20]. Besides, the electrode materials such as transition-metal oxides, LDHs, sulfides, carbides, nitrides, etc. have been reported as the battery-type electrode which stores the charge via sluggish faradic redox reactions [21]. Recently, LDHs attract major attention because of their tunable elemental composition, large ion accessibility, high surface area and faster ion exchange. Apart from this, LDHs exhibit oxygen vacancies that accelerate fast ion exchange by creating the midgap electronic states [22]. However, the poor electrical conductivity of the pristine LDHs hinders their direct application in the supercapacitor [23]. In the literature, a variety of different LDHs based supercapacitive electrodes have been reported which can be classified as pristine LDHs, carbon-LDHs composites, LDHs metal-based composites and others.

3.1.1. Pristine LDHs

The $Co(OH)_2$ and $Ni(OH)_2$ have been reported as the best battery-type electrode for hybrid supercapacitor, however, the reported specific capacities are much lower than the theoretical values (2076 C g^{-1} [24] and 1040 C g^{-1} [25] respectively). The binary CoNi LDH shows improved performance over single systems by combining the advantages of both cobalt and nickel. Recently, pristine CoNi LDHs have been prepared with a variety of different nanostructured forms for

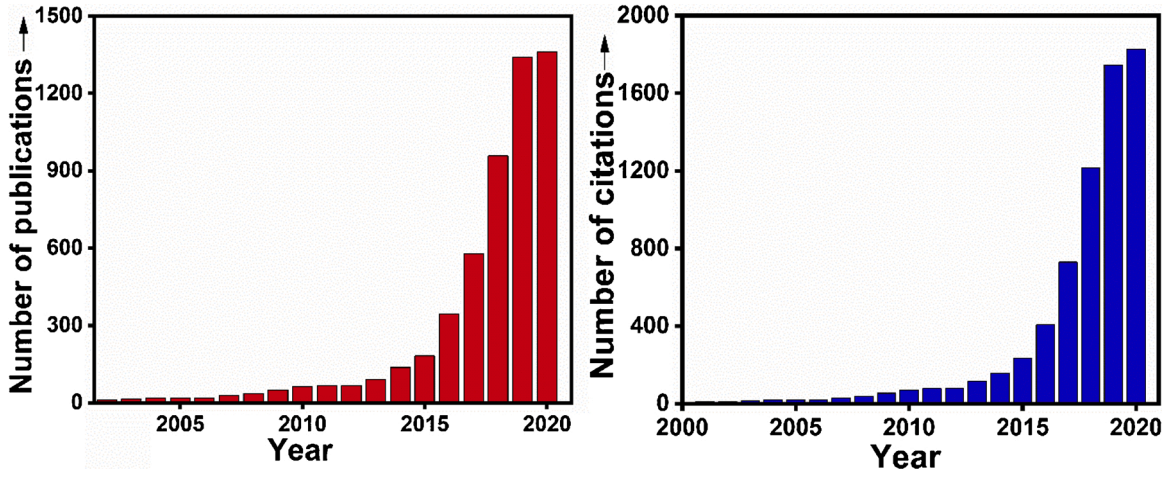

Fig. 1. Histogram for (A) the number of publications and (B) the number of citations for electrodeposited LDHs in the last 20 years.

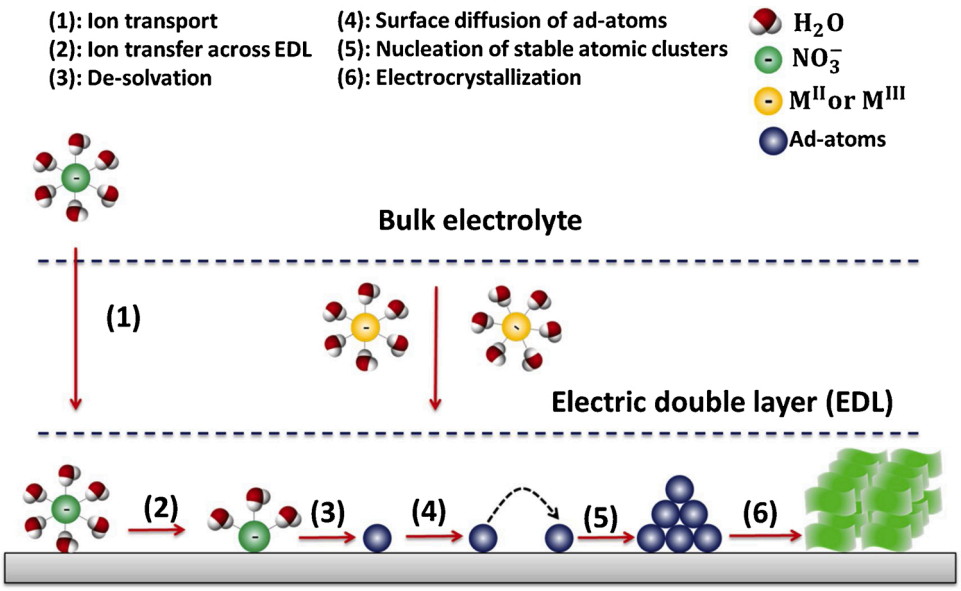

Fig. 2. Schematic diagram of nucleation and growth processes in electrodeposited LDHs.

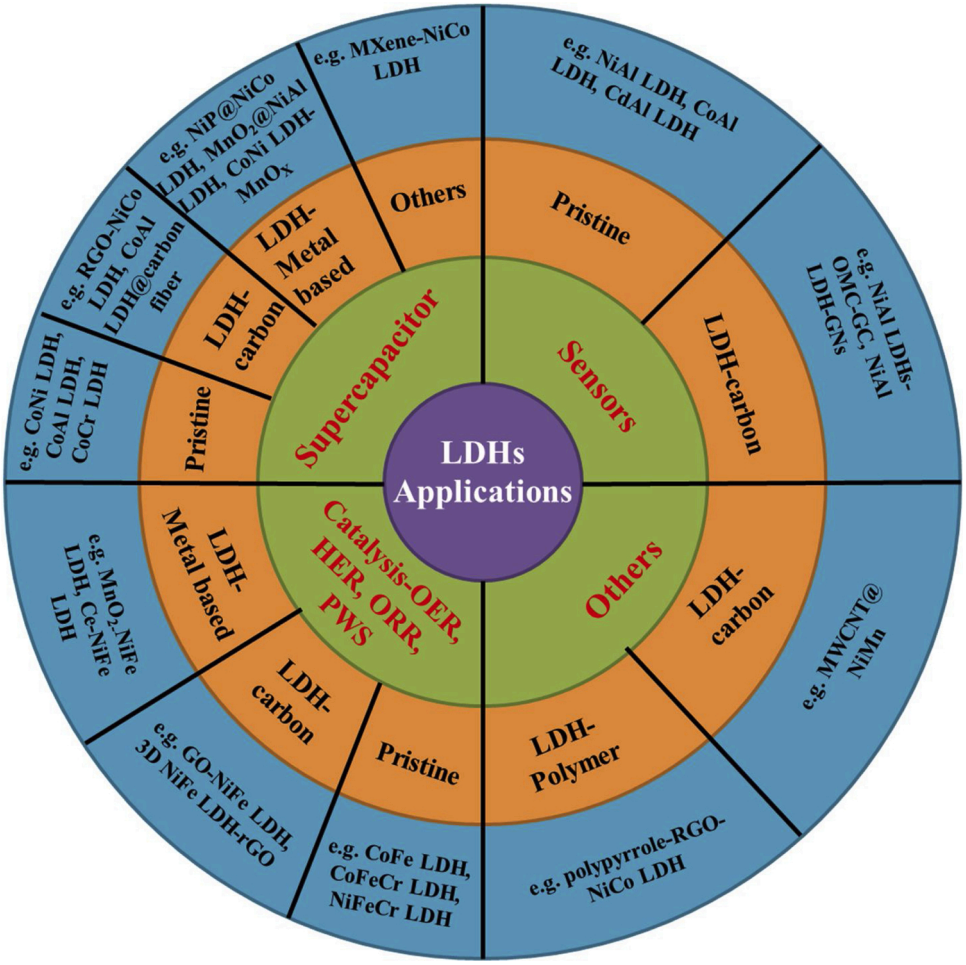

Fig. 3. Classifiactions of electrodepositited LDHs-based materials.

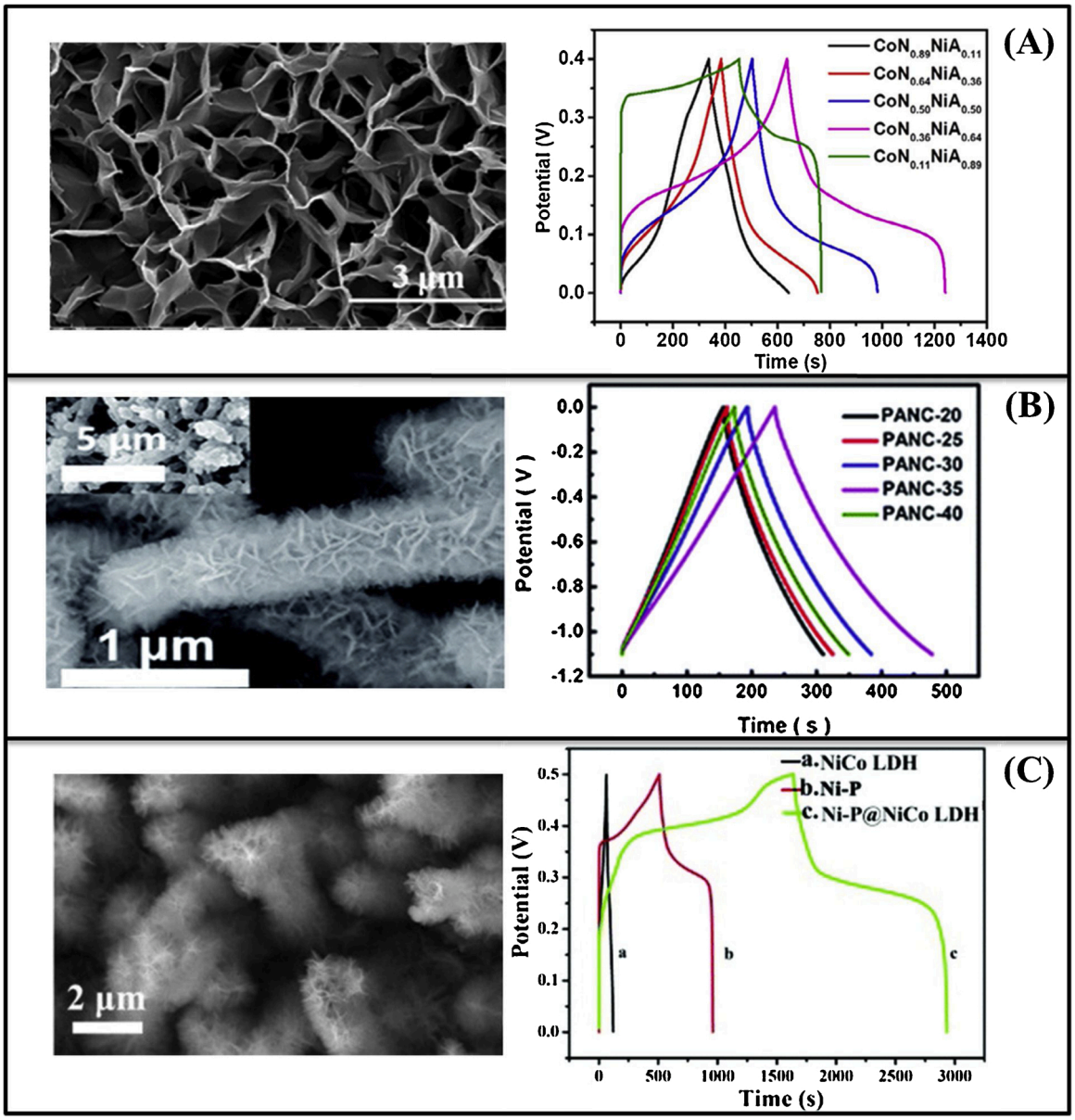

Fig. 4. FESEM image and GCD curves of (A) CoNi LDH, reproduced with permission from Ref. [26], (B) PANC-CoNi LDH, reproduced with permission from Ref. [43] and (C) Ni-P-NiCo LDH, reproduced with permission from Ref. [57].

supercapacitor applications. Wei et al. [26] fabricated the CoNi LDH on nickel foam via facile potentiodynamic electrodeposition method in the potential window of 0–1.1 V vs SCE. The nanostructure of CoNi LDH was controlled by varying different molar compositions between Co and Ni, such as 0.89:0.11, 0.64:0.36, 0.50:0.50, 0.34:0.64 and 0.11 M:0.89 M, respectively and their corresponding electrochemical performances were evaluated. The SEM image of $CoN_{0.36}$:$NiA_{0.64}$ is shown in Fig. 4A, depicting the network-like structure comprised of many interconnected nanosheets. As calculated from the GCD curve (Fig. 4A), owing to the synergic effect, the $CoN_{0.36}$:$NiA_{0.64}$ electrode showed a maximum specific capacity of 606 C g^{-1} (1515 Fg^{-1}) at 1 A g^{-1}. Authors claimed that the enhanced performance of the $CoN_{0.36}$:$NiA_{0.64}$ electrode was attributed to the integrated structure of the nanosheets which shorten the proton diffusion distance and the ultrathin nanosheets, providing more electrochemically active sites for redox reactions. Also, the higher interlayer distance (8.43 Å) facilitates a fast redox process and better accessibility of the reactant. Furthermore, the hybrid supercapacitor was fabricated by using $CoN_{0.36}$:$NiA_{0.64}$ as the positive electrode and the activated carbon (AC) as the negative electrode ($CoN_{0.36}$:$NiA_{0.64}$//AC). This device showed an energy density of 34.5 Wh kg^{-1} at 425 W kg^{-1} with excellent stability of 85.4 % after 5000 GCD cycles. In another study, to overcome the limited rate capability and the reversibility of a $Co(OH)_2$ film electrode, Jagadale et al. [27] synthesized CoMn LDH via potentiostatic electrodeposition method at a constant potential of −1.0 V vs Ag/AgCl. In their work, the molar ratios between Co:Mn were optimized. The CoMn LDH prepared at a molar ratio of 1:9 showed a maximum specific capacity of 849 C g^{-1} (1062 F g^{-1}) at the scan rate of 5 mV s^{-1}. When the Mn^{2+} concentration was reduced in the CoMn LDHs, the interplanar spacing was enhanced due to repulsive interaction between hydroxide planes. Furthermore, the hybrid supercapacitor (CoMn LDH//AC) showed a maximum energy density of 4.4 Wh kg^{-1} at a power density of 2500 W kg^{-1} with appreciable stability of 84.2 % after 5000 GCD cycles. Similarly, a variety of different pristine LDHs such as CoNi [28], CoAl [29,30], CoCr [31], CoMn [27,32], CoNi [33,34] NiCo [35–40] and NiCoFe LDH [41] have been prepared via electrodeposition method on conducting substrate for supercapacitor applications.

3.1.2. LDH-carbon composites

Besides the excellent electrochemical activity of LDHs, they are morphologically unstable over cycles and have low electrical conductivity. Also, the pristine LDHs show inferior rate capability owing to the poor mass diffusion and electron transfer through the electrode. These issues can be rectified by combining them with conducting and high surface area carbon electrodes such as activated carbon, carbon nanotubes, graphene, etc. For example, Jiang et al. [42] prepared NiCo LDH/3D reduced graphene oxide (RGO) composite electrode on nickel foam for supercapacitors. The NiCo LDH was deposited galvanostatically at various temperatures on the dip-coated GO substrate at a constant current of 8 mA for 20 min. The FESEM image showed the formation of vertically aligned nanosheets with an average thickness of 10 nm. This composite (NF@RGO/NiCo LDH) electrode deposited at 20 °C showed a maximum capacity of 1163 C g^{-1} (1454.2 F g^{-1}) at the current density of 1 A g^{-1} with capacitance retention of 73.5 % after 5000 GCD cycles. Authors claimed that the enhanced performance of this composite electrode is attributed to the thinner nanoflakes with good conductivity. The hybrid supercapacitor was fabricated by combing this composite positive electrode with a negative nitrogen-doped reduced graphene oxide electrode that showed a maximum energy density of 57.5 Wh kg^{-1} at a power density of 900 W kg^{-1}. This device also retained the excellent stability of 98.3 % at the current density of 10 A g^{-1} after 10,000 cycles.

Apart from graphene, carbon materials such as 1D carbon nanotubes (CNT) and multiwalled carbon nanotubes (MWCNT) have been considered promising electrodes for supercapacitors due to their higher length-diameter ratio and excellent electronic conductivity. However, they are prepared with sophisticated, expensive and complex techniques. Recently, novel 1D carbon materials have been prepared via facile and simple protocols. For instance, Cao et al. [43] derived a 1D carbon nanowire from potentiodynamically deposited PANI coating which was further loaded by CoNi LDH *via* electrodeposited. As shown in the FESEM image (Fig. 4B), CoNi LDH was vertically grown on carbon wires. The deposition time and deposition cycles were optimized (Fig. 4B). This optimized composite electrode showed a maximum specific capacity of 1070 C g^{-1} (1529.52 F g^{-1}). It was claimed that the superior performance of the optimized electrode was attributed to N-doped nanowires, offering descent wettability and conductivity for depositing CoNi LDH with a large surface area. Also, the core-shell structured electrode shortens the electron transport distance, reducing the charge transfer resistance. The hybrid supercapacitor showed the maximum energy density of 38.73 Wh kg^{-1} at the power density of 0.92 kW kg^{-1} along with the stability of 85.17 % after 10,000 cycles. Similarly, a variety of different composite electrodes has been prepared and tested for supercapacitor application, for instance, NiFe LDHs/nickel foam-rGo [44], CoAl LDH-carbon fiber [45], CoNi LDH-Au-ErGO [46], PANI derived carbon-CoNi LDH, ZnO-C-CoNi LDH [47], cobalt carbonate-NiCo LDH [48], NiCo LDH-rGO@nickel foam [49], NiCo LDH-bucky paper [50], $Ni_xCo_{1-x}(OH)_2$ ErGO [51], NiCo LDH-CFC [52], $Ni_xCo_{1-x}(OH)_2$-carbon nanofoam [53], NiAl LDH-rGO [54] and NiCo LDH-rGO [55].

3.1.3. LDH-metal based composites

The electrical conductivity and electrochemically active sites of LDHs can be enhanced by combing them with metal chalcogenides (metal oxides, sulfides, and selenides) and metal phosphides. Commonly, binary metal sulfides having narrow band gaps and higher electrical conductivity shows higher electrochemical performance. Many reports have been made on the fabrication of binary metal sulfides in different nanostructures with severe agglomeration as a drawback. To overcome these drawbacks, Xin et al. [56] fabricated the NiCo sulfide-NiCo LDH composite and its supercapacitor performance was evaluated. The NiCo LDH was deposited at different durations (10, 20, 40 and 80 s) on the Ni foam containing hydrothermally grown NiCo sulfide to fabricate the core-shell structure electrode. Morphological studies depict that increase in the deposition time increases the deposition amount of NiCo LDH. The LDH deposited at 80 s filled the pores between the nanotubes which affects the electron transport. The LDH deposited at 40 s exhibited the optimum morphology for the electrochemical performance. The NiCo LDH deposited at 40 s showed a maximum specific capacity of 1263 C g^{-1} (2105 F g^{-1}) with capacitance retention of 65.1 % after 3000 GCD cycles which were higher than the capacitance retention of NiCoS. Authors claimed that this enhanced performance was owing to the hierarchical porous structure and chemical bonding between the NiCoS and NiCo LDH, enhancing the charge transport process between the active components and the current collector and thereby contributing to the superior rate capability. The practical applicability of NiCoS- NiCo LDH electrode was evaluated by fabricating an asymmetric device using activated carbon as a negative electrode and NiCoS-NiCo LDH as a positive electrode. The device showed a maximum energy density of 23.73 Wh kg^{-1} at a power density of 400 W kg^{-1}.

Recently, Xing et al. [57] prepared NiP via phosphorization of nickel foam on which NiCo LDH was deposited using a potentiodynamic method. As shown in the FESEM image (Fig. 4C), NiCo LDH was conformally coated on the nanorods of NiP. The loading amount of NiCo LDH was controlled by varying deposition cycles. The optimized composite (NiCo LDH@NiP) electrode showed a maximum specific capacity of 2609 C g^{-1} (2899.5 F g^{-1}) at the current density of 2.5 A g^{-1} with a stability of 96 % after 10,000 cycles. Authors claimed that this enhanced performance was attributed to the highly exposed and fully utilized active sites and small charge transfer resistance of the electrode. The hybrid supercapacitor formed with activated carbon as a negative electrode showed a maximum energy density of 35.1 Wh kg^{-1} at a power density of 770.8 W kg^{-1} and the stability of 70 % after 5000 GCD cycles. Similarly, different LDH/metal-based composite electrodes have been reported for supercapacitor application, including MnO_2-NiAl LDH [58], NiP-CoAl LDH [59], CoNi LDH-MnO_X [9], MnO_2-NiAl LDH, $CuCo_2S_4$--$NiCo(OH)_2$ [60], $NiCo_2O_4$-$NiCo(OH)_2$ [61], NiCo LDH-Mn_3O_4 [62], NiCo-NiCo LDH [63], S-doped NiCo LDH [64], CuO-ZnCo LDH [65], $NiCu(OH)_2$-NiCuSe [66], CuO/NiCo LDH [67] and $Ni_xCo_{2x}(OH)_y$-Ni/ITO [68].

3.1.4. Other LDH based electrodes

Recently, MXenes have gained great interest in various electrochemical applications owing to their high surface area, layered structure, high conductivity and chemical stability. For instance, Li et al. [69] prepared a Ti_3C_2-NiCo LDH composite electrode for supercapacitor application. The NiCo LDH was deposited *via* a potentiodynamic method on the Ti_3C_2 drop cast Ni foam. The composite was prepared with various MXene to LDH ratios. The electrode prepared at the ratio of 3:2 showed a maximum specific capacity of 589 C g^{-1} (984 F g^{-1}) at the current density of 2 A g^{-1} with capacitance retention of 76 % after 5000 GCD cycles. Authors claimed that the enhanced performance of the composite electrode was ascribed to the good conductivity of MXene, supporting the effective charge transfer and preventing the agglomeration over cycling. The hybrid supercapacitor was fabricated using multiwalled carbon nanotube coated nickel foam as a negative electrode which showed a maximum energy density of 36.70 Wh kg^{-1} at the power density of 1.44 kW kg^{-1}. The electrodeposition parameters and supercapacitive performances of the LDHs-based electrodes are summarized in Table 1.

3.2. LDHs in catalysis

3.2.1. Electrocatalysis

Electrodeposited pristine LDHs and their composites have been reported as effective catalysts in different processes such as oxygen evolution reaction (OER), hydrogen evolution reaction (HER), oxygen reduction reaction (ORR), urea electrolysis and oxidation of methanol. Electrocatalysts are imperative in the field of electrochemical water splitting (OER and HER) and metal-air batteries (OER and ORR). In the water splitting, at an anode, the water is split into the oxygen gas along

Table 1
Deposition parameters and supercapacitive performance of LDHs reported so far (PT-Potentiostatic, PD- Potentiodynamic and GS- Galvanostatic).

Deposition parameters				Supercapacitive performance						
Material	Mode of deposition	Deposition bath	Deposition parameter	Electrolyte	Potential window	Specific capacity (C g^{-1})	Specific energy (Wh Kg^{-1}) at specific power (W Kg^{-1})	Cell configuration	Cell potential (V)	Ref.
CoNi LDH-MnO_X	PT	$Co(NO_3)_2$ (0.08 M) + Ni $(NO_3)_2$ (0.02 M)	−0.9 V vs. SCE	1 M KOH	−0.2 to 0.5 V vs. SCE	1022	28.1 at 400	CoNi LDH-MnO_X//AC	1.6	[9]
CoNi LDH	PD	$Co(NO_3)_2$+ $Ni(OAc)_2$ (0.1 M)	0 to −1.1 V vs. SCE	1 M KOH	0 to 0.4 V vs. SCE	606	34.5 at 425	$CoN_{0.36}$ $NiA_{0.64}$ @NF//AC	1.8	[26]
CoMn LDH	PT	$Co(NO_3)_2.6H_2O$ (0.045 M) +$Mn(NO_3)_2.6H_2O$ (0.005 M)	−1.0 V vs. Ag/AgCl	1 M LiOH	−0.2 to 0.6 V vs. Ag/AgCl	849	4.4 at 2500	CoMn LDH@Ni foam //AC	1.8	[27]
CuO-CoNi LDH	PD	$Co(NO_3)_2.6H_2O$ (0.01 M)+ Ni $(NO_3)_2.6H_2O$ (0.04 M)	−0.1 to 0.4 V vs. SCE	2 M KOH	−0.2 to 0.6 V vs. SCE	319 mAh g^{-1}	92.5 at 400	CuO-CoNi LDH//RGO	1.6	[28]
CoAl LDH	GS	$CoSO_4$·7H2O (0.266 M) + H_3BO_3 (0.04 M)	−1.5 mA	1 M KOH	−0.1 to 0.5 V vs. Ag/AgCl	0.510 F cm^{-2}	–	–	–	[29]
CoAl LDH	PT	[$Co(NO_3)_2$+ $Al(NO_3)_3$](0.03 M)+ KNO_3 (0.3 M)	−0.9 V vs. SCE	1 M KOH	0 to 0.6 V vs. SCE	300	–	–	–	[30]
CoCr LDH	PT	$Co(NO_3)_2·6H_2O$ + Cr $(NO_3)_3·9H_2O$	−1.2 V vs. Hg/HgO	1 M KOH	−0.1 to 0.5 V vs. Hg/HgO	125	14.2 at 4860	CoCr LDH//RGO	1.6	[31]
CoMn LDH@CFP	PT	$KMnO_4$ (0.001 M) + Co $(NO_3)_2$ (0.099 M)	− 0.9 V vs. SCE	1 M KOH	−0.3 to 0.3 V vs. SCE	980	19.1 at 400 Wkg^{-1}	CoMn LDH@CFP//AC@CFP	1.6	[32]
$Co_{1-x}Ni_x$ LDH	PD	0.1 M of $Co(NO_3)_2$+ $Ni(NO_3)_2$	−1.2 to 0 vs. SCE	1 M KOH	−0.2 to 0.5 V vs. SCE	849	–	–	–	[33]
CoNi $(OH)_2$	PT	$Ni(NO)_2.6H_2O$ (0.0025 M)+ $Co(NO)_2.6H_2O$ (0.0075 M) + CH_4N_2S (0.002 M)	−2 V vs. Ag/AgCl	2 M KOH	0 to 0.6 V vs. Ag/AgCl	790	21.3 at 3625	$Co_{0.75}Ni_{0.25}$ $(OH)_2$//AC	1.4	[34]
$Ni(OH)_2$-$Co(OH)_2$	PT	$Ni(NO_3)_2$ (0.05 M) + Co $(NO_3)_2$ (0.05 M)	− 1.1 V vs. SCE	1 M KOH	−0.2 to 0.6 V vs. SCE	609	101.3 at 0.2	The carbon nanofoam paper //$Ni(OH)_2$-$Co(OH)_2$	1.8	[35]
NiCo LDH	Pulsed electrodeposition	$Ni(NO_3)_2·6H_2O$ (0.76 M) +Co $(NO_3)_2·6H_2O$ (0.34 M)	1.0 V vs. Ag/AgCl	1 M KOH	0 to 0.5 V vs. Ag/AgCl	1094	4.1 at 4000	NiCo LDH//AC	0.8	[36]
NiCo LDH @NF	PT	$NiSO_4·6H_2O$ (0.005 mol L^{-1}) $CoSO_4·6H_2O$ (0.01 mol L^{-1}) + CH_4N_2S (0.06 mol L^{-1})	−1.0 V vs. Ag/AgCl	2 M KOH	0−0.6 V vs. Hg/HgO	705	29.1 at 903.1	NiCo LDH@NF//AC	1.6	[37]
NiCo LDH @NF	GS	0.01 M of $Ni(NO_3)_2·6H_2O$ + $Co(NO_3)_2·6H_2O$	−1 mA cm^{-2}	1 M KOH	0 to 0.5 V vs. Hg/HgO	2725	–	–	–	[38]
3D NiCo LDH @NF	GS	0.01 mol·L^{-1} of Ni $(NO_3)_2·6H_2O$ + Co $(NO_3)_2·6H_2O$	–0.5 mA·cm^{-2}	6M KOH	0 to 0.6 V vs. Hg/HgO	1056	103.0 at 3.0	3D NiCo LDH@NF// Ketjenblack	1.5	[39]
NiCo LDH-MOF	PT	$Ni(NO_3)_2·6H_2O$ (0.01 M) + $Co(NO_3)_2·6H_2O$ (0.01 M)	−1.1 V vs. SCE	3 M KOH	−0.2 to 0.45 V vs. SCE	837.85	57.8 at 748.7	NiCo LDH-MOF//AC	1.5	[40]
NiCoFe LDH	PT	$Ni(NO_3)_2·6H_2O$ (0.06 M) + $Co(NO_3)_2·6H_2O$ (0.02 M) + $Fe(NO_3)_3·9H_2O$ (0.02 M)	−0.94 V vs. SCE	1 M KOH	0 to 0.6 V vs. Hg/HgO	792.6	73.07 at 1.07	NiCoFe LDH//AC	1.6	[41]
NF@RGO- NiCo LDH	GS	$Ni(NO_3)_2·6H_2O$ (0.29 g) + Co $(NO_3)_2·6H_2O$ (0.58 g) + NH_4Cl (1.07 g)	8 mA (20 min)	1 M KOH	0 to 0.8 V vs. SCE	1163	57.5 at 900	NF@RGO- NiCo LDH// NF@N-RGO	1.8	[42]
PANI Derived Carbon-CoNi LDH	PT	$CoCl_2.6H_2O$ (0.15 M) + Ni $(NO_3)_2.6H_2O$ (0.15 M)	–1.0 V	6M KOH	−0.3 to 0.4 V	1070	38. at 0.92	PANC-CoNi LDH//PANC	1.4	[43]
NiFe LDH- rGo@NF	PT	$Ni(NO_3)_2.6H_2O$ (0.001 M) +$Fe(NO_3)_3.9H_2O$ (0.004 M)	−1.2 V vs. SCE	2 M KOH	0 to 0.5 V vs. SCE	731	17.71 at 348.49	NiFe LDHs-rGO@NF// MC/NF	1.6	[44]
CoAl LDH@carbon fiber	PT	$Co(NO_3)_2·6H_2O$ (0.1 M) +Al $(NO_3)_3·9H_2O$ (0.005 M)	−1.1 V vs. Ag/AgCl	2 M KOH	0 to 1 V vs. Ag/AgCl	634	–		–	[45]
CoNi LDHs@Au@ErGO	PT	$Co(NO_3)_2.6H_2O$ (1.455 g) + $Ni(NO_3)_2.6H_2O$ (2.91 g)	−1.0 V	2 M KOH	0 to 0.5 V	20.15 m F cm^{-1}	–	–	–	[46]
ZnO-C- CoNi LDH	PT	$CoCl_2·6H_2O$ (1.78 g) +Ni $(NO_3)_2·6H_2O$ (2.18 g)	–1.0 V vs. SCE	1 M KOH	0 to 0.4 V vs. SCE	6.2578 F cm^{-2}	1.078 Wh cm^{-3} at 0.02 W cm^{-2}	ZnO-C-CoNiLDH//Fe_2O_3	1.6	[47]
Cobalt carbonate-NiCo LDH	–	$Co(NO_3)_2·6H_2O$ (0.004 M) + $Ni(NO_3)_2·6H_2O$ (0.002 M)	–	2 M KOH	−0.2 to 0.8 V vs. Hg/HgO	7.71 F cm^{-2}	–	–	–	[48]

(*continued on next page*)

Table 1 (*continued*)

Deposition parameters				Supercapacitive performance						
Material	Mode of deposition	Deposition bath	Deposition parameter	Electrolyte	Potential window	Specific capacity (C g^{-1})	Specific energy (Wh Kg^{-1}) at specific power (W Kg^{-1})	Cell configuration	Cell potential (V)	Ref.
NiCo LDH-rGO@NF	PD	CTAB (0.01 g) + Co $(NO_3)_2.6H_2O$ (0.29 g) + Ni $(NO_3)_2$. $6H_2O$ (0.145 g)	0.0 to -1.5 V vs. Ag/AgCl	3M NaOH	−0.2 to 0.8 V vs. Ag/AgCl	2133	68 at 1070 W kg^{-1}	NiCo LDH-CTAB-rGO@NF//rGO@NF	1.5	[49]
NiCo LDH@BP	PT	$Ni(NO_3)_2$ (0.1 M) + $Co(NO_3)_2$ (0.03 M)	−1.0 V vs. SCE	2 M KOH	−0.2 to 0.5 V vs. SCE	1.5 F cm^{-2}	–	NiCo LDH@BP//BP	1.4	[50]
$Ni_xCo_{1-X}(OH)_2$-ErGO	Pulsed PT	$Ni(NO_3)_2.6H_2O$ (0.003 M)+ $Co(NO_3)_2{\cdot}6H_2O$ (0.006 M)	−0.8 to −1.2 V vs. Ag/AgCl	1 M KOH	−0.2V to 0.5 V vs. SCE	96 mA h g^{-1}	–	–	–	[51]
NiCo LDH-CFC	GS	$Ni(NO_3)_2{\cdot}6H_2O$ (0.0036 M) + $Co(NO_3)_2{\cdot}6H_2O$ (0.0009 M) + NH_4Cl (0.01 M)	10 mA	1 M KOH	−0.2 to 0.6 V vs. SCE	1232	37 at 800	NiCo LDH//rGO	1.6	[52]
$Ni_{0.33}Co_{0.67}$ $(OH)_2$@carbon nanofoam	PT	(0.1 M)[$Ni(NO_3)_2$ + Co $(NO_3)_2$]	−1.1 V vs. SCE	1 M KOH	−0.4 to 0.7 V vs. SCE	1.52 C cm^{-2}	490 mWh cm^{-2} at 154 mW h cm^{-2}	$Ni_{0.33}Co_{0.67}$ $(OH)_2$ //CNFP	2	[53]
NiAl LDH-rGO	PD	$Ni(NO_3)_2.6H_2O$ (0.01 M) + Al $(NO_3)_3.6H_2O$ (0.005 M)	0.0 to -1.2 V vs Ag/AgCl	3M KOH	−0.1 to 0.6 V vs. Ag/AgCl	1885	76.23 at 1599.51	NiAl LDH-rGO//Fe_2O_3-rGO	1.6	[54]
NiCo LDH-rGO@NF	PT	($Ni(NO_3)_2$ (0.036 mol dm^{-3}) + $C_4H_6CoO_4$ (0.064 mol dm^{-3})	−0.1 V vs. SCE	2 mol dm^{-3} KOH	0 to 0.5 V vs. Hg/HgO	5.820 C cm^{-2}	45.83 at 396.15	NiCo LDH-rGO@NF//AC	1.4	[55]
NiCoS-NiCo LDH	PT	$Ni(NO_3)_2{\cdot}6H_2O$ (0.002 M) + $Co(NO_3)_2{\cdot}6H_2O$ (0.004 M)	−1.2 V vs. SCE	3M KOH	0 to 0.6 V vs. Hg/HgO	1263	23.73 at 400	NiCoS-NiCO LDH//AC	1.6	[56]
NiP-NiCo LDH	PD	(0.004 M) [$Co(NO_3)_2$ + Ni $(NO_3)_2$]	−0.5 to -1.1 V vs. SCE	6M KOH	−0.1 to 0.8 V vs. Hg/HgO	2609	35.1 at 770.8	NiP-NiCoLDH//AC	1.6	[57]
MnO_2-NiAl LDH	PT	$NiCl_2{\cdot}$ $6H_2O$ (0.03 M)+ $AlCl_3$ (0.01 M) + KNO_3 (0.15 M) + $KMnO_4$ (0.02 M)	−0.9 V vs. SCE	6M KOH	−0.2 to 0.8 V	1554	–	–	–	[58]
NiP-CoAl LDH	PD	$Co(NO_3)_2$ (0.0075 M) + Al $(NO_3)_3$ (0.0025 M) + KNO_3 (0.1 M)	50 mV s^{-1} (20 cycles)	2 M KOH	0 to 0.6 V vs. Hg/HgO	556	37.18 at 450	NiP-CoAl LDH//AC	1.6	[59]
$CuCo_2S_4$- NiCo $(OH)_2$	PT	$NiCl_2.4H_2O$ (0.01 M) + Co $(NO_3)_2{\cdot}6H_2O$ (0.01 M) + KNO_3 (0.1 M)	−1.0 V vs SCE	3M KOH	−0.1 to 0.6 V vs. SCE	1638	32 at 750	$CuCo_2S_4$-NiCo $(OH)_2$// $CuCo_2S_4$-NiCo $(OH)_2$	1.5	[60]
$NiCo_2O_4$-NiCo LDH	PT	0.1 mol L^{-1} of $Ni(NO_3)_2{\cdot}6H_2O$ + $Co(NO_3)_2{\cdot}6H_2O$	−1.0 V vs. Ag/AgCl	6.0 M KOH	0 to 0.5 V vs. Ag/AgCl	1379	–	–	–	[61]
NiCo LDH-Mn_3O_4	PT	$Ni(NO_3)_2.$ $6H_2O$ (0.0005 M) + $Co(NO_3)_2.6H_2O$ (0.001 M)	1.0 V vs. Ag/AgCl	3M KOH	−0.1to 0.5 V vs. Ag/AgCl	1034	9681.6 at 20.98	NiCo LDH-Mn_3O_4//AC	1.5	[62]
NiCo-NiCo LDH	GS	0.002 M of $NiSO_4{\cdot}6H_2O$ + $CoSO_4{\cdot}7H_2O$	4 mA cm^{-2}	1 M NaOH	−0.2 to 0.6 V vs. SCE	1931	100 at 1500	NiCo-NiCo LDH NTAs//CNFs-CFC	1.5	[63]
S-doped NiCo LDH	PD	$Co(OAc)_2$ + $NiCl_2$ + $C_4H_6CoO_4$	−1.20 to 0.20 V vs. Ag/AgCl at 5 mV s^{-1}	6M KOH	0 to 0.50 V vs. Ag/AgCl	344	–	–	–	[64]
CuO-ZnCo LDH	PT	$Zn(NO_3)_2{\cdot}6H_2O$ (0.067 M) + $Co(NO_3)_2{\cdot}6H_2O$ (0.133 M) + H_2O_2 (0.067 M)	−1.0 V vs. Ag/AgCl	6M KOH	0–0.5 V vs. Hg/HgO	2.634 C cm^{-2}	22.10 at 434	CuO-ZnCo LDH//Carbon	1.5	[65]
NiCu LDH-Ni-Cu-Se	PT	$Ni(NO_3)_2$ (0.1 M)+$Cu(NO_3)_2$ (0.1 M) + CH_4N_2O (0.4 M)	−1.0 V vs SCE	1 M KOH	0 to 0.7 V vs. Ag/AgCl	184	–	–	–	[66]
NiO-NiCo LDH	PT	(0.1 M)[$Ni(NO_3)_2{\cdot}6H_2O$ + Co $(NO_3)_2{\cdot}6H_2O$]	−1 V vs Ag/AgCl	3M KOH	0 to 0.5 V vs. Ag/AgCl	938	–	–	–	[67]
Ni_xCo_{2x} $(OH)_y$ @Ni@ITO	PT	$Ni(NO_3)_2.$ $6H_2O$ (0.002 M) + $Co(NO_3)_2$ $6H_2O$ (0.004 M)	1.0 V vs. Ag/AgCl)	0.1 M KOH	0.25 to 0.6 V vs. Ag/AgCl	92.4 m F cm^{-2}	–	–	–	[68]
NiCo LDH@MXene	PD	0.01 M $Co(NO_3)_2.6H_2O$ (0.01 M) + $Ni(NO_3)_2.6H_2O$ (0.005 M)	−1.2 V to 0.2 V vs. Ag/AgCl	6M KOH	0 to 0.6 V vs. SCE	589	36.70 at 1440	MXene-NiCo LDH@NF//MWCNT@NF	1.6	[69]

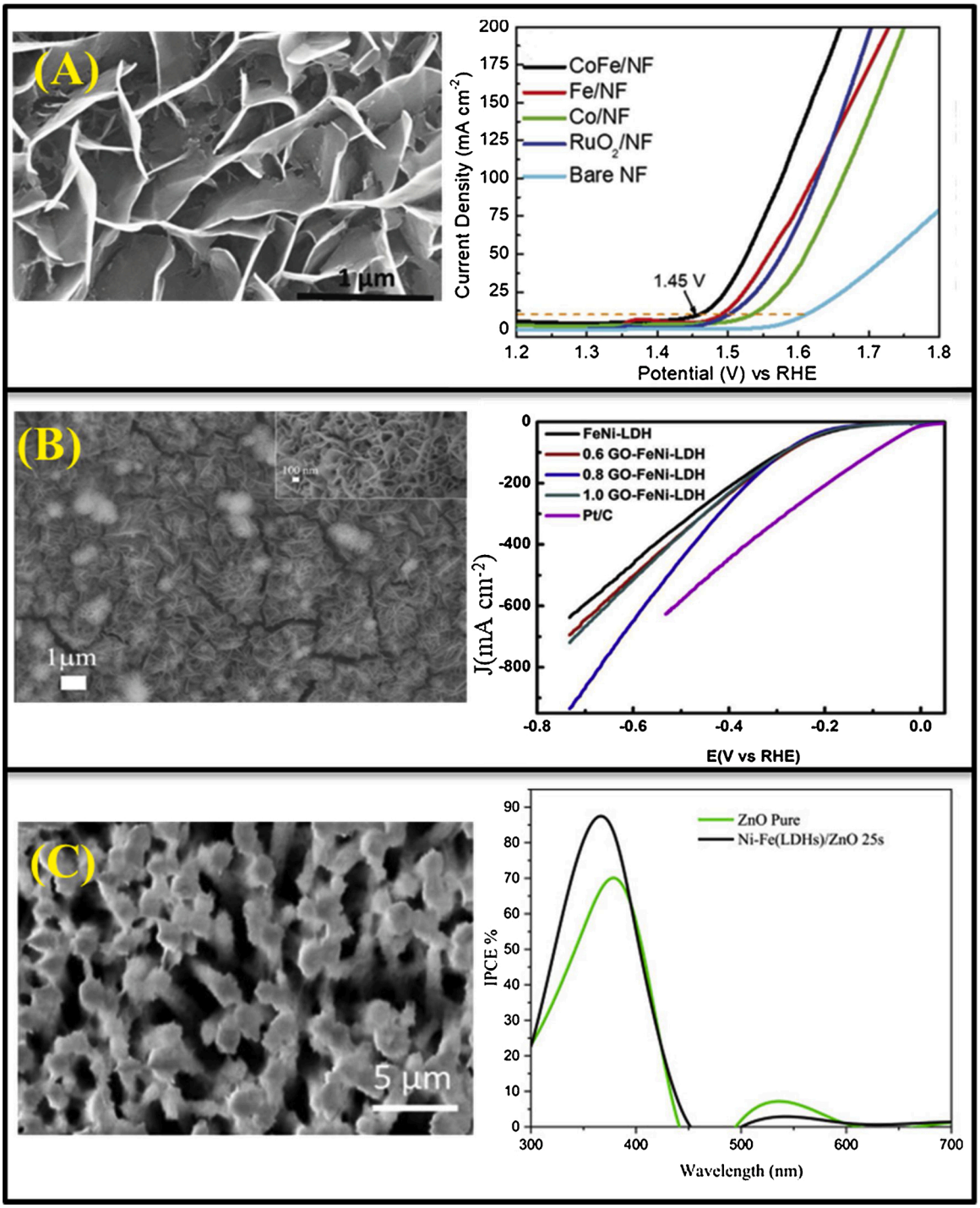

Fig. 5. FESEM image and catalytic performance of (A) CoFe LDH, reproduced with permission from Ref. [75], (B) GO-NiFe LDH, reproduced with permission from Ref. [98] and (C) NiFe LDH-ZnO, reproduced with permission from Ref. [102].

with electrons and protons. At a cathode, protons and electrons combine to form hydrogen gas. The produced gas can be used as an energy source for various applications. Commonly, Pt-group metals and Ir/Ru-based materials are used as the catalyst for HER and OER, respectively. These materials are costly and scarce that leads to a search for new catalysts. Among numerous efforts to find alternate catalysts, pristine LDHs and their composites are frequently reported as electrocatalysts for water splitting [70]. In the case of metal-air batteries, the energy is produced by the redox reaction between the metal and the oxygen. The ORR is sluggish and slower than the metal reduction process, resulting in lower power output capability and round trip efficiency. To overcome these problems, catalysts can be employed to accelerate the ORR activity [71–73]. The electrodeposited LDHs and their composites reported for different electrocatalytic activities are discussed below.

3.2.1.1. Oxygen evolution reaction (OER). In the process of water splitting, the OER seems to be arduous owing to its sluggish kinetics, attributing to a four-electron multi-step reaction as shown in Eq. (3).

$$2H_2O \rightarrow O_2 + 4H^+ + 4e^- \quad (3)$$

The catalyst not only accelerates the OER activity but also lowers the overpotential value [74]. Recently, CoFe LDH has attracted major

attraction owing to its abundance, high conductivity, cost-effectiveness and enhanced electrocatalytic activity. For instance, Babar et al. [75] electrodeposited the CoFe LDH on a nickel foam and its catalytic performance was compared with the bare nickel and single hydroxide systems, such as $Co(OH)_2$ and $Fe(OH)_2$. This deposited CoFe LDH showed a lower overpotential of 220 mV to achieve a current density of 10 mA cm^{-2} and the Tafel slope value of 40 mV dec^{-1}. The overpotential and Tafel slope values were found to be smaller than bare nickel and single hydroxide systems as shown in Fig. 5A. The prepared sample showed potential retention of 92 % after 50 h. The polarization curves before and after stability also support the stability of the CoFe LDH. The electrochemically active surface area of the CoFe LDH film catalyst was found to be 1665 cm^{-2} which was higher than the $Co(OH)_2$ and $Fe(OH)_2$. Authors claimed that the lower value of contact angle of the CoFe LDH enhances the interaction between the electrode and the electrolyte and thereby the catalytic activity [76–78]. Previously, different pristine LDHs have been reported, including CoNi LDH [79], CoFeCr LDH [80], CoMn LDH [81], NiFe LDH [82–86], 2D NiFeCo LDH/nickel foam [87], NiFeCr LDH [88], ZnCo LDH [89] and NiFeAl LDH [90]. The performance of pristine LDHs is far away from the expectation due to lower surface area and poor electrical conductivity. To overcome these issues, pristine LDHs can be combined with conducting and high surface area materials, such as graphene, carbon nanotubes and MXenes. For instance, Hu et al. [91] Prepared MXene (Ti_3C_2)-CoNi LDH composite catalysts at different weight ratios for OER activity. In the preparation of CoNi LDH, the molar ratio of 1:1 between Co and Ni was found to be superior as compared to their single hydroxide systems ($Co(OH)_2$ and $Ni(OH)_2$). The composite (Ti_3C_2-CoNi LDH) made with a weight ratio of 1:4 showed a lower overpotential of 257.4 mV with a Tafel slope of 68 mV dec^{-1}. Authors claimed that the Ti_3C_2-CoNi LDH composite lowers the binding energy of the intermediates and boosts the electron transfer, enhancing the OER activity. In another study, Yu et al. [92] synthesized NiFe LDH-electrochemically reduced graphene oxide (ErGO) composite for OER activity. The overpotential of 3D ErGO-NiFe LDH was found to be 1.489 V. Authors claimed that this finest performance is attributed to the synergic effect of the NiFe LDH nanoplates and 3D interpenetrated network structure of graphene, offering the excellent OER activity. Similarly, different electrodeposited LDHs based electrodes have been reported for OER activity, such as $Cu(OH)_2$-NiFe LDH [93], MnO_2-NiFe LDH [94], Ce-NiFe LDH [95], NiFe LDH-Ni-Ni mesh [96], Pt_3Ni_1-Ni_XFe [97] and 3D GO-NiFe LDH [98].

3.2.1.2. Hydrogen evolution reaction (HER). Like other evolution reactions, the HER requires significant overpotential, therefore, it is imperative to find high-performance electrocatalysts to maximize the process efficiency. The HER reaction occurs on the cathode as follows,

$$H^+ + e^- \rightarrow H_{ads} \quad (4)$$

$$2H_{ads} \rightarrow H_2 \quad (5)$$

$$H_{ads} + H^+ + e^- \rightarrow H_2 \quad (6)$$

In the HER, at first, the Volmer reaction takes place, in which, the electron from the surface of the electrode absorbs the proton from the electrolyte to form an intermediate adsorbed hydrogen atom as shown in the Eq. (4). In the second stage, two possible reactions take place namely Tafel reactions or Heyrovsky reactions (Eqs. (5) and (6)) to liberate hydrogen [99]. Recently, many efforts have been made to replace the conventional noble metal catalysts. Among them, electrodeposited LDHs are widely investigated. For example, Jadhav et al. [95] electrodeposited the Ce doped NiFe LDH to be used as HER catalyst. The NiFe LDH was deposited from the electrolyte containing Ni:Fe in the ratio of 1:1 and Ce was used to partially replace Fe such as $NiFe_{1-x}Ce_x$, where x = 0, 0.1, 0.2 or 0.3 respectively. The $NiFe_{0.8}Ce_{0.2}$ showed the lowest overpotential of 147 mV with a lower Tafel slope of 112 mV dec^{-1}. Authors claimed that the improved performance was attributed to the Ce doping which alters the morphology and enhances the conductivity of the NiFe LDH. In another work, Han et al. [98] synthesized the 3D GO-NiFe LDH composite for effective water splitting. Composites were prepared by adding different concentrations of graphene oxide in the electrodeposition bath, such as 0, 0.6, 0.8 and 1.0 mg mL^{-1}. As shown in Fig. 5B, a composite prepared at GO concentration of 0.8 mg mL^{-1} shows regular arrays with vertically grown interconnected thin sheets, facilitating more active sites and fast electron transfer. This optimized composite electrode (0.8GO-NiFe LDH) showed excellent HER activity with a smaller overpotential of 0.119 V to attain the current density of 10 mA cm^{-2}. The smaller Tafel slope value of 36 mV dec^{-1} indicates the fast kinetics of the catalytic activity which was attributed to the well-arranged morphology as shown in the SEM image. The GO prevents the formation of aggregated nanosheets, enhancing the kinetics and stability of the material. The chronoamperometric study showed appreciable stability of 95.5 % after 25 h. The authors claimed that this study may give new insight to construct the bifunctional novel LDH composites for electrochemical water splitting. Similarly, composites like NiCo LDH C-doped-*N*-doped carbon [100], 2D NiFeCo LDH@NF [87], sulfur-doped NiCo LDH@SS [64] and NiFe LDH-3D porous Ni@Ni mesh [96] have been reported. The electrodeposition parameters of LDHs-based electrocatalysts and their catalytic (OER and HER) performances are summarized in Table 2.

3.2.1.3. Oxygen reduction reaction (ORR). In fuel cells, the ORR plays a predominant role in which oxygen is reduced by protons and electrons to produce water as shown in Eq. 7.

$$\frac{1}{2}O_2 + 2H^+ + 2e^- \rightarrow H_2O \quad (7)$$

Platinum (Pt) has been reported as an ideal electrocatalyst for ORR but it requires high mass loading which made its applicability difficult on large scale. To prepare less expensive and efficient electrocatalysts, researchers prepared various Pt alloys, core-shell structures, transition metal oxides and chalcogenides and carbon-based non-noble metal composite catalysts [101]. The layered structure and high surface area of LDHs attracted researchers to develop the LDH based electrocatalyst for ORR. Yu et al. [97] integrated the PtNi nanoparticles with the NiFe LDH nanosheets (PtNi-Ni_XFe LDH) as the electrocatalyst for ORR. The molar ratio between the Pt and Ni was optimized by varying the different molar ratios, such as 4:0, 3:1, 1:1 and 1:3, respectively and their catalytic activity was evaluated. The Ni^{2+} vacancy can be created in the LDH to alter the electronic structure and stabilize the PtNi nanoparticles. The sample in which Pt and Ni in the ratio of 3:1 (Pt_3Ni_1-Ni_XFe LDH) showed the more positive half-wave potential of 0.852 V. The anchoring of Pt-Ni alloy modulated the electronic catalytic property of Ni_XFe LDH which enhances the catalytic performance. The stability of Pt_3Ni_1-Ni_XFe was evaluated by LSV curves which showed a negligible decrease of current density after 20 h. Authors claimed that Ni vacancy in the LDH supports the uniform formation of Pt-Ni alloy, enhancing the conductivity and providing more active sites for ORR.

3.2.2. Photochemical water splitting (PWS)

A PWS is a clean and renewable strategy to store chemical energy (hydrogen and oxygen) using sunlight. The conduction band of the semiconductor should be more negative with respect to the hydrogen reduction potential which results in hydrogen gas and the valance band should be more positive than the oxidation potential of water that results in oxygen gas. The ZnO is a commonly reported catalyst for PWS owing to its wide bandgap and electron mobility. However, under the influence of UV rays, a pristine ZnO dissolves in aqueous media, deteriorating the catalytic performance. Many techniques have been developed to overcome this issue, such as ion implementation, dye sensitization, doping, etc. LDHs are active substitutes due to their layered structure, flexibility in composition, controlled dimension, low cost, and ease of synthesis. Recently, Mustafa et al. [102] electrodeposited NiFe LDH on

Table 2
Deposition parameters and catalytic performance of electrodeposited LDHs reported so far (PT-Potentiostatic, PD- Potentiodynamic and GS- Galvanostatic).

Electrodeposition parameters				Electrocatalytic performance				
Oxygen Evolution Reaction (OER) catalytic activity								
Material	Mode of deposition	Deposition bath	Deposition parameter	Electrolyte	Over potential (mV)	Tafel slope (mV dec^{-1})	Stability	Ref.
CoFe LDH	PT	$Co(No_3)_2{\cdot}6H_2O$ (0.003 M)+Fe $(NO_3)_3{\cdot}$ $9H_2O$ (0.003 M)	−1 V vs. SCE	1 M KOH	220	40	92 % (50 h@10 mA cm^{-2})	[75]
CoFe LDH	PT	$Co(NO_3)_2$ (0.006 M) + $Fe(NO_3)_3$ (0.006 M)	−1.42 V vs. Hg/Hg_2SO_4	O_2 saturated 1 M KOH	280	28		[76]
CoFe LDH	PT	$Co(NO_3)_2{\cdot}6H_2O$ (0.15 M) + $FeSO_4{\cdot}7H_2O$ (0.15 M)	−1 V vs. SCE	1 M KOH	250	35	–	[77]
CoFe LDH	PT	[$FeCl_2.4H_2O$ + $CoCl_2.6H_2O$](0.1 M)	–	1 M NaOH	286	48		[78]
CoNi LDH@NF	PT	$Co(NO_3)_2$ (0.3 M) + $Ni(NO_3)_2$ (0.2 M)	−1 V vs. Ag/AgCl	1 M KOH	366	65	92.6% (10 h@1 V vs. Ag/AgCl)	[79]
CoFeCr LDH	PT	$Co(NO_3)_2{\cdot}6H_2O$ (0.00048 M)+Fe $(NO_3)_3{\cdot}9H_2O$ (0.00048 M)+Cr $(NO_3)_3{\cdot}9H_2O$ (0.00024 M)	−1 V vs. Ag/AgCl	1 M KOH	270	–	–	[80]
CoMn LDH	PT	$Co(NO_3)_2{\cdot}6H_2O$ (0.01 M)+Mn $(CH_3COO)_2{\cdot}6H_2O$ (0.05 M) + Na_2SO_4 (0.01 M)	−1 V vs. Ag/AgCl	0.1 M KOH	258	49	99.5% (1000 CV cycles @50 mV s^{-1})	[81]
NiFe LDH	GS	$NiSO_4{\cdot}6H_2O$ (0.008 M)+$FeSO_4{\cdot}7H_2O$ (0.008 M)+$(NH_4)_2SO_4$ (0.025 M)	10 mA cm^{-2}	0.75 M Na_2CO_3/$NaHCO_3$ + 2 M NaOH	260	29		[82]
NiFe (oxy) hydroxide	GS	[$Ni(NO_3)_2.6$ H_2O + $FeCl_2.4$ H_2O](0.1 M)	−10 mA cm^{-2}	1 M KOH	250			[83]
NiFe LDH	PT	$NiSO_4{\cdot}6H_2O$ (60 g L^{-1})+$FeSO_4{\cdot}6H_2O$ (8.6 g L^{-1})+H_3BO_3 (30 g L^{-1})+NaCl (25 g L^{-1})	−7 V vs. Ag/AgCl	1 M KOH	260	55.6	–	[84]
NiFe Oxides-(Oxy) hydroxides	PT	$[Ni(bpy)_3](BF_4)_2$ (0.001 M) in 1 M KOH	0.7 V vs. NHE	1 M KOH	232	51.1	–	[85]
NiFe $(OH)_2$	PT	$Ni(NO_3)_2$ (0.003 M)+$Fe(NO_3)_3$ (0.003 M)	−1.0 V vs. SCE	1 M KOH	–	65		[86]
2D NiFeCo LDH@NF	PD	$NiCl_2.6H_2O$ (0.01 M) + $FeCl_2.6H_2O$ (0.01 M) + $CoCl_2.6H_2O$ (0.0001 M)	−0.4 to −1.3 V vs. SCE	1 M KOH	210	39		[87]
NiFeCr $(OH)_2$	PT	$Ni(NO_3)_2{\cdot}6H_2O$ (0.003 M) + Fe $(NO_3)_3{\cdot}9H_2O$ (0.003 M) + Cr $(NO_3)_3{\cdot}6H_2O$ (0 to 0.004 M)	−1.0 V vs. Ag/AgCl	1 M KOH	200	29		[88]
ZnCo LDH	PT	[$ZnSO_4{\cdot}7H_2O$+ $CoSO_4{\cdot}7H_2O$] (0.2 M)	−1.0 V vs. Ag/AgCl	0.1 M KOH	427	59		[89]
D-NiFeAl LDH	PT	$Ni(NO_3)_2.6H_2O$ (0.003 M) + Fe $(NO_3)_3.9H_2O$ (0.003 M)	−1.0 V vs. SCE	1 M KOH	262	41.67		[90]
CoNi LDH - $Ti_3C_2T_x$ MXene	PT	[$Ni(NO_3)_2{\cdot}6H_2O$ + $Co(NO_3)_2{\cdot}6H_2O$] (18 M)	−1.1 V vs. Ag/AgCl	1 M KOH	257	68		[91]
3D NiFe LDH-ErGO	PT	[$Ni(NO_3)_2.6H_2O$ + $Fe(NO_3)_3.9H_2O$] (0.05 M)	–1.2 V vs. SCE	O_2 saturated 1 M KOH	259	39	90% (2 h @1.49 V vs. RHE)	[92]
$Cu(OH)_2$-NiFe LDH	PT	$Ni(NO_3)_2$ + $FeSO_4$	−1.2 V vs. Ag/AgCl	1 M KOH	283	88		[93]
MnO_2-NiFe LDH	GS	$Ni(NO_3)_2$ (0.15 M)+ $FeSO_4$ (0.15 M)	5 mA cm^{-2}	1 M KOH	226	200		[94]
Ce-NiFe LDH	PT	$Ni(NO_3)_2.6H_2O$+ $Fe(NO_3)_2.9H_2O$	−1.0 V vs. Ag/AgCl	1 M KOH	175	59		[95]
NiFe LDH@3D Ni@Ni mesh	GS	$Ni(NO_3)_2$ + $FeSO_4$	5 mA cm^{-2}	O_2 saturated 1 M KOH	190	108		[96]
Pt_3Ni_1-NixFe	PT	$Ni(NO_3)_2{\cdot}6H_2O$ (0.03 M) + Fe $(NO_3)_3{\cdot}9H_2O$ (0.01 M)	1.0 V vs. Ag/AgCl	1 M KOH	265	22.2		[97]
GO-FeNi-LDH	PD	$Ni(NO_3)_2.6H_2O$ (0.0015 M) + $FeCl_2.4H_2O$ (0.0015 M) + $FeCl_3.6H_2O$ (0.003 M) + GO	−1.156 to 0.244 V vs. SCE @ 2 mV s^{-1}	1 M KOH	210	33		[98]
Hydrogen evolution reaction (HER) catalytic activity								
S-NiCo LDH	PD	$Co(OAc)_2$ +$NiCl_2$ + $C_4H_6CoO_4$	−1.20 to 0.20 V vs. Ag/AgCl	6M KOH	70	69		[64]
CoFe $(OH)_2$	PT	$Co(NO_3)_2{\cdot}6H_2O$ (0.003 M)+Fe $(NO_3)_3.9H_2O$ (0.003 M)	−1 V vs. SCE	1 M KOH	110	35		[75]
2D NiFeCo LDH@NF	PD	$NiCl_2.6H_2O$ (0.01 M) + $FeCl_2.6H_2O$ (0.01 M) + $CoCl_2.6H_2O$ (0.0001 M)	−0.4 to −1.3 V vs. SCE	1 M KOH	1.1 V vs. SCE	55		[87]
Ce-NiFe LDH	PT	$Ni(NO_3)_2.6H_2O$ + $Fe(NO_3)_2.9H_2O$	−1.0 V vs. Ag/AgCl	1 M KOH	147	112	82 % (50 h@20 $mAcm^{-2}$)	[95]
NiFe LDH@3D Ni@Ni mesh	GS	$Ni(NO_3)_2$ + $FeSO_4$	5 mA cm^{-2}	1 M KOH	132	107.7	–	[96]
GO-FeNi LDH	PD		−1.156 to 0.244 V vs. SCE @ 2 mV s^{-1}	1 M KOH	285	36		[98]

(*continued on next page*)

Table 2 (*continued*)

Electrodeposition parameters				Electrocatalytic performance				
Oxygen Evolution Reaction (OER) catalytic activity								
Material	Mode of deposition	Deposition bath	Deposition parameter	Electrolyte	Over potential (mV)	Tafel slope (mV dec^{-1})	Stability	Ref.
$NiCo_3$ LDH C-doped NSs@NC	PT	$Ni(NO_3)_2.6H_2O$ (0.0015 M)+ $FeCl_2.4H_2O$ (0.0015 M)+$FeCl_3.6H_2O$ (0.003 M) + GO $Co(NO_3)_2{\cdot}6H_2O$ (0.087 g) + Ni $(NO_3)_2{\cdot}6H_2O$ (0.087 g) + SDS (0.01 g)	−1.0 V vs. SCE	1 M KOH	99	43		[100]

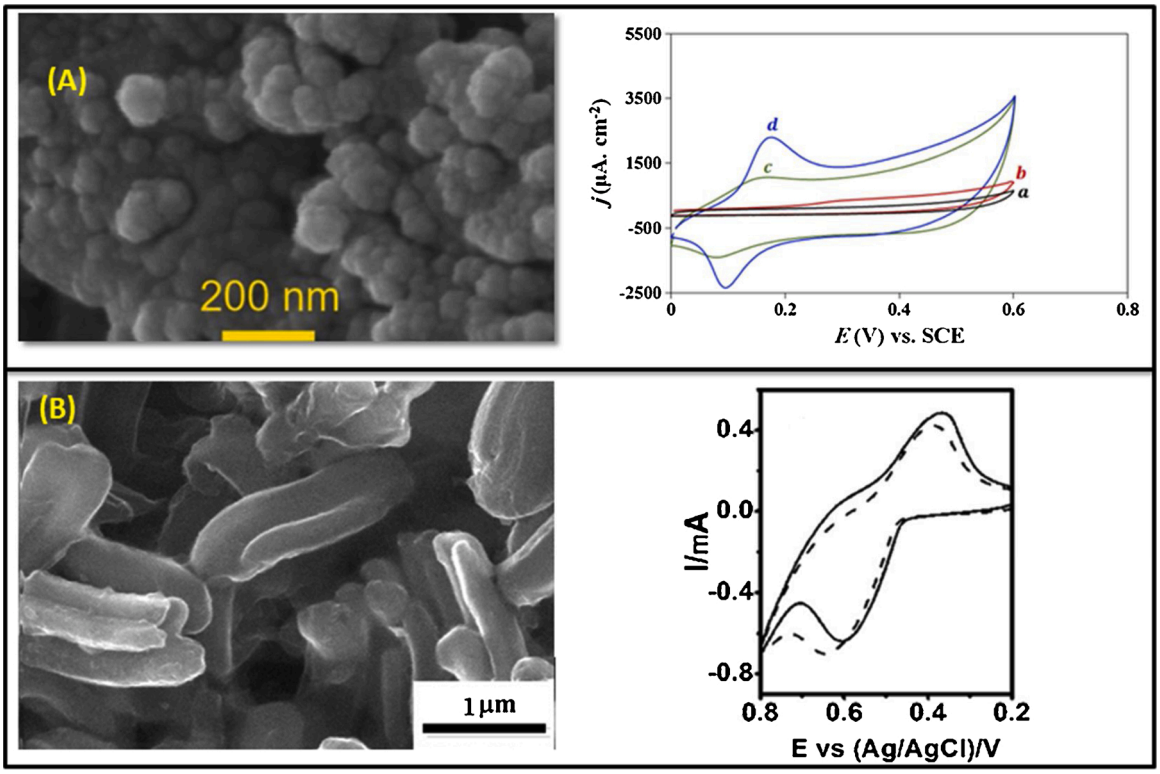

Fig. 6. FSEM image and sensing prrformance of (A) CoAl LDH, reproduced with permission from Ref. [109] and (B) NiAl LDH-OMC, reproduced with permission from Ref. [113].

hydrothermally grown ZnO nanorods for photocatalytic application. As shown in Fig. 5C, the NiFe LDH is uniformly coated on the ZnO nanorods. The incident monochromatic photon to current conversion efficiency (IPCE) of 82 % was obtained for NiFe LDH-ZnO deposited at 25 s at the maximum wavelength of 380 nm which is higher than that of pristine ZnO (Fig. 5C). Authors claimed that the composite with NiFe LDH deposited for 25 s showed fast and stable photoresponse due to the chemical coupling and synergic effect, facilitating the lowest redox potential for the oxidation of water. Composites such as $BiVO_4$-rGO-NiFe LDH [103], α-Fe_2O_3-NiFe LDH [104], TiO_2-ZnFe LDH [105] and ZnCo LDH-α-Fe_2O_3 [106] have also been reported for PWS application.

3.2.3. Other catalytic activities of LDHs

Apart from water splitting and metal-air batteries, electrodeposited LDHs and their composites have also been reported for different chemical oxidation and electrolysis. For instance, Wang et al. [107] electrodeposited a NiAl LDH on the glassy carbon electrode for methanol oxidation. The molar ratios between Ni and Al were varied as 2:1, 3:1 and 4:1 and the optimized ratio was found to be 3:1. They concluded that the efficiency of the catalyst can be improved by altering the Ni:Al molar ratios and the concentration of KOH. In another study, Qian et al. [16] prepared a pristine and sulfur-doped CoNi LDH on the stainless steel (SS) and indium tin oxide (ITO) to evaluate the catalytic activity for methanol oxidation. As compared with undoped CoNi LDH, an S-doped LDH showed an onset potential of 0.45 V for methanol oxidation with improved stability. Some other catalysts have also been reported, such as NiAl LDH-graphene hybrid for dopamine oxidation [108] and 2D NiFeCo LDH@nickel foam for urea electrolysis [87].

3.3. LDHs in sensors

LDHs are mainly used in electrochemical sensors, a type of sensor that uses electrodes as a transducer element. These sensors have gained great interest owing to their low cost and fast analysis. Morphological and electrochemical properties of electrodeposited LDHs and their composites extend their applicability in the field of biosensors. These are the devices used to detect the presence or the concentration of a biological analyte (biomolecule, microorganism, etc.).

3.3.1. LDHs in biosensors

Heidari et al. [109] electrodeposited nanoparticles CoAl LDH on pencil graphite electrode (PGE) for the electrochemical sensing of L-cysteine which is a key factor in the diagnosis of various diseases (Fig. 6A). As shown in CV curves (Fig. 6A), the addition of L-cysteine increased the anodic and cathodic peaks of CoAl LDH, confirming the redox process of L-cysteine catalyzed by the CoAl LDH. The authors concluded that the CoAl LDH-PGE shows a wide range (100 pM–0.1 μM) and a low detection limit (100 pM) for sensing L-cysteine. Due to the low detection limit, CoAl LDH-PGE based sensors may show accuracy in biological environments, pharmaceutical samples, and other industries with appreciable repeatability. In another study, gold nanoparticles composited with electrodeposited NiAl LDH were also reported as an effective sensing electrode with a low detection range (10 μM–1.0 mM) and good selectivity [110]. Lactate is associated with different clinical diseases such as septic shocks, metabolic disorder and oxygenation state of tissues. Therefore, there has been great attention to developing a lactate sensor. Carpani et al. [111] electrodeposited the NiAl LDH on the surface of the platinum electrode and employed it for lactate detection. The quantization of lactate was done using chronoamperometry at −0.35 V vs. SCE which measures the oxidation current generated by the hydrogen peroxide produced from the enzymatic conversion of lactate into pyruvate. The film stabilized by Nafion membrane was employed to determine the lactate in the bovine serum sample.

Graphene nanosheets (GNs) are well known for their exceptional thermal and mechanical properties, high surface area, and high electrical conductivity. Liang et al. [112] electrodeposited the NiAl LDH nanoparticles on the GNs *via* a co-electrodeposition approach for the detection of methyl parathion. The LDH-GNs composite combines the properties of both LDH and GNs to show excellent sensing and selectivity with the detection limit of 0.6 mg mL^{-1}. The sensor produced using this device showed good reproducibility and stability.

Similarly, Ju et al. [113] prepared an ordered mesoporous carbon (OMC)-NiAl LDH composite electrode for non-enzymatic acetylcholine (ACh) sensor. As shown in Fig. 5B, the pristine OMC showed the rod-like structure on which NiAl LDH was deposited (Fig. 6B). As shown in the CV curve (Fig. 6B), the addition of ACh increases the anodic peak with a slight decrement in the cathodic peak which was attributed to the typical oxidation process. The detection limit was found to be 4922 μm, higher than the previous reports. This composite electrode showed high sensitivity, excellent stability and a low detection limit for detecting ACh. Shishegari et al. [114] deposited the Pd-NiAl LDH on the nitrogen-doped functionalized graphene for glucose sensing. The sensor showed a lower detection limit of 234 nM with a sensitivity of 315.46 μA $cm^{-2}dec^{-1}$. Authors claimed the enhanced performance attributed to the active centers of Ni and Pd, facilitating a greater electron transfer process.

3.3.2. LDHs in other sensors

The pH is commonly measured in a laboratory which is an important parameter in some chemical and biological processes. Recently, Mignani et al. [115] developed a pH sensor using electrodeposited CoAl LDH on a glassy carbon electrode. The CoAl LDH electrode showed a fast response time of 5 s throughout all ranges of pH and was not affected by interferences from the common cations as well as redox processes. Anthracene is a polycyclic aromatic hydrocarbon (PAH) that is a globally distributed highly toxic contaminant. Researchers developed various methods to detect the PAH, for instance, Qiao et al. [116] electrodeposited CdAl LDH at different periods (50, 100, 200 and 300 s) for the voltammetric detection of anthracene. The detection limit for anthracene was evaluated to be as low as 5 fM. It is seen from the above description that, apart from the biosensing applications, electrodeposited LDHs and their composites can be used for other important sensing applications. Deposition parameters of LDHs reported for different sensors are summarized in Table 3.

4. Other applications

Apart from the above-mentioned literature, electrodeposited LDHs and their composites have also been reported for other applications. For instance, LDHs can be grown on the surface of metals for protecting them from corrosion. He et al. [117] coated vanadate loaded ZnAl LDH on the aluminum alloy (AA2024) to avoid corrosion. In vanadate-loaded LDHs, vanadate enhances the barrier property of LDH and enriches corrosion sites to actively protect aluminum. Authors claimed that the electrodeposited LDH with thin coating offered excellent protection as compared to hydrothermally prepared LDH. Similarly, Yin et al. [118] have prepared the zeolitic imidazolate framework-8-PVDF-ZnAl LDH composite electrode to prevent corrosion in Mg alloy. This composite facilitated the superhydrophobicity with a contact angle greater than 150°, protecting the Mg alloys from mechanical wear as well as chemical corrosion.

Although fluorine is an essential micronutrient for the human body, an excess intake of fluorine leads to dental and skeletal fluorosis. Many materials have been investigated for the removal of excessive fluorine from the water, LDHs are also amongst them. Yang et al. [119] prepared the MWCNT-NiMn LDH composite by combining electrodeposition and drop-casting method for the defluoridation. In the composite, MWCNTs act as electron collectors, enhancing the conductivity of the LDH. The MWCNT-NiMn LDH exhibited a high ion exchange quantity (135.1 mg/g from the Langmuir model) with excellent recyclability (92.4 % capability retention after 5 cycles). This composite can be incorporated in the electrochemically switched ion permselective (ESIP) system for continuous separation of F^- with high efficiency. Authors claim that the MWCNT-NiMn LDH could be a promising material for the effective separation of F^-. In another study, Wang et al. [120] prepared the

Table 3
Deposition parameters of electrodeposited LDHs for sensor application reported so far (PT-Potentiostatic, PD- Potentiodynamic and GS- Galvanostatic).

Material	Mode of deposition	Deposition bath	Deposition parameter	Applications	Reference
CoAl LDH	PT	0.03 mol L^{-1} of $Co(NO_3)_2$ +$Al(NO_3)_3$ (Co and Al in the ratio 3:1)	−0.9 V vs SCE	L-cysteine sensor	[109]
Au nanoparticles- NiAl LDH	PT	22.5 mM $Ni(NO_3)_2$ + 7.5 mM $Al(NO_3)_3$	−0.9 V vs SCE	L-cysteine sensor	[110]
NiAl LDH @ platinum surface	PT	0.0225 M $Ni(NO_3)_2$ +0.0075 M $Al(NO_3)_3$ + 0.3 M KNO_3	−0.9 V vs SCE	Lactate biosensor	[111]
NiAl LDH-grpahene	PD	0.3 M KNO_3 + 22.5 mM $Ni(NO_3)_2$ +7.5 mM $Al(NO_3)_2$	0.1 to −1.4 V vs SCE	Detection of methyl parathion	[112]
NiAl LDH-ordered mesoporous carbon	PT	0.060 M $Ni(NO_3)_2$ + 0.015 M $Al(NO_3)_3$ + 1.2 M KNO_3	−0.9 V vs Ag/AgCl	acetylcholine sensor	[113]
N-doped graphene-NiAl LDH	PT	1 mM $PdCl_2$ + 0.12 M $Ni(NO_3)_2$ + 0.04 M $Al(NO_3)_3$ + 0.5 M HNO_3 + 0.15 M KNO_3	−0.9 V vs Ag/AgCl	Glucose sensor	[114]
Glassy carbon coated with CoAl LDH	PT	0.03 M $Co(NO3)_2$ + $Al(NO3)_3$ + 0.3 M KNO_3	−1 V vs SCE	pH sensor	[115]
CdAl LDH	PT	0.0225 M Cd $(NO_3)_2$ + 0.0075 M Al $(NO_3)_3$ + 0.3 M KNO_3	−0.9 V vs Ag/AgCl	Detection of anthracene	[116]

Table 4
Deposition parameters of electrodeposited LDHs for other applications reported so far (PT-Potentiostatic, PD- Potentiodynamic and GS- Galvanostatic).

Material	Mode of deposition	Deposition bath	Deposition parameter	Applications	Reference
CoAl LDH	PD	12.5 mmol L^{-1} $Zn(NO_3)_2{\cdot}6H_2O$ +7.5 mmol L^{-1} $Al(NO_3)_3{\cdot}9H_2O$	−1.3 to −1.8 V vs Ag/AgCl	Corrosion protection	[117]
ZnAl LDH	PT	3 mM $Zn(NO_3)_2{\cdot}6H_2O$ + 3 mM $Al(NO_3)_3{\cdot}9H_2O$	−1 V vs Ag/AgCl	Corrosion protection	[118]
MWCNTs-NiMn LDH	PT	0.075 M $Ni(NO_3)_2$ + 0.025 M $Mn(NO_3)_2$	−1 V vs Ag/AgCl	Defluoridation	[119]
PPy-rGO-NiCo LDH	PT	0.075 M $Ni(NO_3)_2{\cdot}6H_2O$ + 0.025 M $Co(NO_3)_2{\cdot}6H_2O$	−1.5 V vs Ag/AgCl	Removal of dilute dodecyl sulfonate ions	[120]
DMPS-CuCr LDH	PT	.075 mol L^{-1} (0.36 g) $Cu(NO_3)_2$ + 0.025 mol L^{-1} (0.20 g) $Cr(NO_3)_3$ + 0.3 mol L^{-1} KNO_3	−1.4 V	Uptake of heavy metals	[121]

polypyrrole-rGO-NiCo LDH composite by the two-step electrodeposition process for the removal of dodecyl sulfonate ions (DS^-) which causes water pollution. It showed DS^- ion exchange capacity of 160.96 mg g^{-1} with the removal percentage of 92.31 % in the aqueous solution with 10 mg L^{-1} DS^- ions at an electrode potential of 0.8 V. It also showed an efficiency of 88.8 % after 10,000 CV cycles. The unique structure facilitates fast ionic and electronic transport, enhancing the ion exchange capacity and diffusion speed of electrons as well as ions in the hybrid film. The heavy metal present in the water causes severe diseases in humans and other species. To adsorb these heavy metals, Shamsayei et al. [121] reported CuCr LDH/2,3-dimercaptopropane sulfonate composite for the adsorption of heavy metals. Authors claimed that the composite exhibits various sites to adsorb heavy metals with excellent selectivity and good adsorbing capacity (2500 mg g^{-1}) of Hg(II). Different applications and deposition parameters of LDHs and their composites are summarized in Table 4.

5. Conclusion and prospects

Low cost, versatility in chemical composition, a wide range of preparation variability, and unique anion exchange and intercalation properties of LDHs made as a promising candidate for energy and environmental applications. In energy-related and sensor applications, aggregation and stacking of LDH nanosheets limit their practical applicability. To overcome these drawbacks, LDHs have been composited with carbon materials and metal chalcogenides/phosphides. In the case of electrodeposited LDHs, composites have been made with the materials which were prepared *via* different methods. There are very few reports in which LDH based composites were fabricated in single-step electrodeposition technique. Therefore, a new strategy to fabricate the LDH based composite via electrodeposition needs to be developed for extending its practical applicability. The resistance between the substrate and the active material is an important parameter that may retard the performance of the material. To reduce the resistance, different substrate materials such as stainless steel, nickel foam, copper foil, graphitic carbon, glassy carbon, etc. have been reported. However, the loading amount of LDHs is limited on such substrates. In the case of electrochemical energy storage applications, a loading amount of active materials on the substrate is crucial to improve the areal and volumetric capacities. Therefore, the utilization of low-cost and scalable scaffold materials such as carbon nanofibers, graphene foam, etc. is highly recommended. Since the electronic and electrochemical properties of LDHs preferable depend on the ratio between divalent and trivalent cations, it must be optimized based on the performance in a particular application. As the exfoliated LDH nanosheets enhance the electrochemical performance, the methodology to exfoliate the electrodeposited nanosheets needs to be developed. These continuous efforts would open new pathways for electrodeposited LDHs for various applications.

CRediT authorship contribution statement

R.C. Rohit: Conceptualization, Methodology, Investigation, Formal analysis, Interpretation, Visualization, Data curation, writing-original draft. **Ajay D. Jagadale:** Conceptualization, Investigation, Data curation, Visualization, Writing - review & editing, Supervision. **S.K. Shinde:** Visualization, Writing - review & editing. **D.-Y. Kim:** Visualization, Supervision.

Declaration of Competing Interest

The authors declare that they have no known competing financial interests or personal relationships that could have appeared to influence the work reported in this paper.

Acknowledgment

ADJ is thankful to the Department of Science and Technology (DST), Govt. of India for financial assistance under the DST INSPIRE Faculty Scheme [DST/INSPIRE/04/2017/002737].

References

[1] G. Mishra, B. Dash, S. Pandey, Layered double hydroxides: a brief review from fundamentals to application as evolving biomaterials, Appl. Clay Sci. 153 (2018) 172–186, https://doi.org/10.1016/j.clay.2017.12.021.
[2] F. Li, X. Duan, Applications of layered double hydroxides, in: X. Duan, D.G. Evans (Eds.), Layered Double Hydroxides, Springer, Berlin, Heidelberg, 2006, pp. 193–223, https://doi.org/10.1007/430_007.
[3] I. Gualandi, M. Monti, E. Scavetta, D. Tonelli, V. Prevot, C. Mousty, Electrodeposition of layered double hydroxides on platinum: insights into the reactions sequence, Electrochim. Acta 152 (2015) 75–83, https://doi.org/10.1016/j.electacta.2014.11.096.
[4] X. Guo, F. Zhang, D.G. Evans, X. Duan, Layered double hydroxide films: synthesis, properties and applications, Chem. Commun. 46 (2010) 5197–5210, https://doi.org/10.1039/C0CC00313A.
[5] Z. Chang, D.G. Evans, X. Duan, C. Vial, J. Ghanbaja, V. Prevot, M. de Roy, C. Forano, Synthesis of [Zn–Al–CO_3] layered double hydroxides by a coprecipitation method under steady-state conditions, J. Solid State Chem. 178 (2005) 2766–2777, https://doi.org/10.1016/j.jssc.2005.06.024.
[6] V. Prevot, N. Caperaa, C. Taviot-Guého, C. Forano, Glycine-assisted hydrothermal synthesis of NiAl-layered double hydroxide nanostructures, Cryst. Growth Des. 9 (2009) 3646–3654, https://doi.org/10.1021/cg900384n.
[7] J. Prince, A. Montoya, G. Ferrat, J.S. Valente, Proposed general sol−gel method to prepare multimetallic layered double hydroxides: synthesis, characterization, and envisaged application, Chem. Mater. 21 (2009) 5826–5835, https://doi.org/10.1021/cm902741c.
[8] J. Liu, J. Song, H. Xiao, L. Zhang, Y. Qin, D. Liu, W. Hou, N. Du, Synthesis and thermal properties of ZnAl layered double hydroxide by urea hydrolysis, Powder Technol. 253 (2014) 41–45, https://doi.org/10.1016/j.powtec.2013.11.007.
[9] S. Tian, C. Zhao, P. Nie, H. Wang, X. Xue, L. Lin, L. Chang, Electrochemical deposition enables freestanding CoNi layered double hydroxide/MnOX electrode with enhanced electrochemical properties for asymmetric supercapacitors, Energy Technol. 7 (2019), 1900680, https://doi.org/10.1002/ente.201900680.
[10] M. Zhao, Q. Zhao, B. Li, H. Xue, H. Pang, C. Chen, Recent progress in layered double hydroxide based materials for electrochemical capacitors: design, synthesis and performance, Nanoscale 9 (2017) 15206–15225, https://doi.org/10.1039/C7NR04752E.
[11] L. Mohapatra, K. Parida, A review on the recent progress, challenges and perspective of layered double hydroxides as promising photocatalysts, J. Mater. Chem. A 4 (2016) 10744–10766, https://doi.org/10.1039/C6TA01668E.
[12] M. Daud, M.S. Kamal, F. Shehzad, M.A. Al-Harthi, Graphene/layered double hydroxides nanocomposites: a review of recent progress in synthesis and applications, Carbon 104 (2016) 241–252, https://doi.org/10.1016/j.carbon.2016.03.057.

[13] X. Li, D. Du, Y. Zhang, W. Xing, Q. Xue, Z. Yan, Layered double hydroxides toward high-performance supercapacitors, J. Mater. Chem. A 5 (2017) 15460–15485, https://doi.org/10.1039/C7TA04001F.

[14] M. Skompska, K. Zarębska, Electrodeposition of ZnO nanorod arrays on transparent conducting substrates–a review, Electrochim. Acta 127 (2014) 467–488, https://doi.org/10.1016/j.electacta.2014.02.049.

[15] Y. Zhang, J. Wang, M. Li, Y. Wang, Incomplete sulfuration of ternary NiCoAl LDHs electrodeposited on Ni foam: an effective strategy to prepare high-performance binder-free electrodes for hybrid supercapacitors, J. Electrochem. Soc. 166 (2019) A98, https://doi.org/10.1149/2.0431902jes.

[16] L. Qian, W. Chen, M. Liu, Q. Jia, D. Xiao, One-step electrodeposition of S-doped cobalt–nickel layered double hydroxides on conductive substrates and their electrocatalytic activity in alkaline media, ChemElectroChem 3 (2016) 950–958, https://doi.org/10.1002/celc.201600022.

[17] M. Shao, R. Zhang, Z. Li, M. Wei, D.G. Evans, X. Duan, Layered double hydroxides toward electrochemical energy storage and conversion: design, synthesis and applications, Chem. Commun. 51 (2015) 15880–15893, https://doi.org/10.1039/C5CC07296D.

[18] F. Nasirpouri, Fundamentals and principles of electrode-position, in: F. Nasirpouri (Ed.), Electrodeposition of Nanostructured Materials, Springer International Publishing, Cham, 2017, pp. 75–121, https://doi.org/10.1007/978-3-319-44920-3_3.

[19] J. Cherusseri, N. Choudhary, K.S. Kumar, Y. Jung, J. Thomas, Recent trends in transition metal dichalcogenide based supercapacitor electrodes, Nanoscale Horiz. 4 (2019) 840–858, https://doi.org/10.1039/C9NH00152B.

[20] J. Wei, X. Li, H. Xue, J. Shao, R. Zhu, H. Pang, Hollow structural transition metal oxide for advanced supercapacitors, Adv. Mater. Interfaces 5 (2018), 1701509, https://doi.org/10.1002/admi.201701509.

[21] Y. Gogotsi, R.M. Penner, Energy storage in nanomaterials – capacitive, pseudocapacitive, or battery-like? ACS Nano 12 (2018) 2081–2083, https://doi.org/10.1021/acsnano.8b01914.

[22] Y. Tang, H. Shen, J. Cheng, Z. Liang, C. Qu, H. Tabassum, R. Zou, Fabrication of oxygen-vacancy abundant NiMn-layered double hydroxides for ultrahigh capacity supercapacitors, Adv. Funct. Mater. 30 (2020), 1908223, https://doi.org/10.1002/adfm.201908223.

[23] J. Fang, M. Li, Q. Li, W. Zhang, Q. Shou, F. Liu, X. Zhang, J. Cheng, Microwave-assisted synthesis of CoAl-layered double hydroxide/graphene oxide composite and its application in supercapacitors, Electrochim. Acta 85 (2012) 248–255, https://doi.org/10.1016/j.electacta.2012.08.078.

[24] X. Ou, Y. Wang, S. Lei, W. Zhou, S. Sun, Q. Fu, Y. Xiao, B. Cheng, Terephthalate-based cobalt hydroxide: a new electrode material for supercapacitors with ultrahigh capacitance, Dalton Trans. 47 (2018) 14958–14967, https://doi.org/10.1039/C8DT03231A.

[25] M. Urso, G. Torrisi, S. Boninelli, C. Bongiorno, F. Priolo, S. Mirabella, $Ni(OH)_2$ @Ni core-shell nanochains as low-cost high-rate performance electrode for energy storage applications, Sci. Rep. 9 (2019) 7736, https://doi.org/10.1038/s41598-019-44285-1.

[26] M. Wei, Q. Huang, Y. Zhou, Z. Peng, W. Chu, Ultrathin nanosheets of cobalt-nickel hydroxides hetero-structure via electrodeposition and precursor adjustment with excellent performance for supercapacitor, J. Energy Chem. 27 (2018) 591–599, https://doi.org/10.1016/j.jechem.2017.10.022.

[27] A.D. Jagadale, G. Guan, X. Li, X. Du, X. Ma, X. Hao, A. Abudula, Ultrathin nanoflakes of cobalt–manganese layered double hydroxide with high reversibility for asymmetric supercapacitor, J. Power Sources 306 (2016) 526–534, https://doi.org/10.1016/j.jpowsour.2015.12.097.

[28] F. Chen, C. Chen, Q. Hu, B. Xiang, T. Song, X. Zou, W. Li, B. Xiong, M. Deng, Synthesis of CuO@CoNi LDH on Cu foam for high-performance supercapacitors, Chem. Eng. J. 401 (2020), 126145, https://doi.org/10.1016/j.cej.2020.126145.

[29] P.Y. Loh, K.K. Lee, Y. Ng, C.H. Sow, W.S. Chin, Co/Al layered double hydroxides nanostructures: a binderless electrode for electrochemical capacitor, Electrochem. Commun. 43 (2014) 9–12, https://doi.org/10.1016/j.elecom.2014.03.001.

[30] E. Scavetta, B. Ballarin, C. Corticelli, I. Gualandi, D. Tonelli, V. Prevot, C. Forano, C. Mousty, An insight into the electrochemical behavior of Co/Al layered double hydroxide thin films prepared by electrodeposition, J. Power Sources 201 (2012) 360–367, https://doi.org/10.1016/j.jpowsour.2011.10.122.

[31] S.K. Kiran, M. Padmini, H.T. Das, P. Elumalai, Performance of asymmetric supercapacitor using CoCr-layered double hydroxide and reduced graphene-oxide, J. Solid State Electrochem. 4 (2016) 927–938, https://doi.org/10.1007/s10008-016-3436-8.

[32] C. Zhao, S. Tian, P. Nie, T. Deng, F. Ren, L. Chang, Electrodeposited binder-free CoMn LDH/CFP electrode with high electrochemical performance for asymmetric supercapacitor, Ionics 26 (2020) 1389–1396, https://doi.org/10.1007/s11581-019-03290-0.

[33] S.B. Kulkarni, A.D. Jagadale, V.S. Kumbhar, R.N. Bulakhe, S.S. Joshi, C. D. Lokhande, Potentiodynamic deposition of composition influenced Co1−xNix LDHs thin film electrode for redox supercapacitors, Int. J. Hydrogen Energy 38 (2013) 4046–4053, https://doi.org/10.1016/j.ijhydene.2013.01.047.

[34] B. Xiao, W. Zhu, Z. Li, J. Zhu, X. Zhu, G. Pezzotti, Tailoring morphology of cobalt–nickel layered double hydroxide via different surfactants for high-performance supercapacitor, R. Soc. Open Sci. 5 (2018), 180867, https://doi.org/10.1098/rsos.180867 (n.d.).

[35] T. Nguyen, M. Boudard, M.J. Carmezim, M.F. Montemor, Layered $Ni(OH)_2$ -Co $(OH)_2$ films prepared by electrodeposition as charge storage electrodes for hybrid supercapacitors, Sci. Rep. 7 (2017) 39980, https://doi.org/10.1038/srep39980.

[36] X. Wang, X. Li, X. Du, X. Ma, X. Hao, C. Xue, H. Zhu, S. Li, Controllable synthesis of NiCo LDH nanosheets for fabrication of high-performance supercapacitor electrodes, Electroanalysis 29 (2017) 1286–1293, https://doi.org/10.1002/elan.201600602.

[37] Y. Wang, Z. Yin, G. Yan, Z. Wang, X. Li, H. Guo, J. Wang, New insight into the electrodeposition of NiCo layered double hydroxide and its capacitive evaluation, Electrochim. Acta 336 (2020), 135734, https://doi.org/10.1016/j.electacta.2020.135734.

[38] J. Xing, S. Wu, K.Y.S. Ng, Electrodeposition of ultrathin nickel–cobalt double hydroxide nanosheets on nickel foam as high-performance supercapacitor electrodes, RSC Adv. 5 (2015) 88780–88786, https://doi.org/10.1039/C5RA17481C.

[39] M. Yang, H. Cheng, Y. Gu, Z. Sun, J. Hu, L. Cao, F. Lv, M. Li, W. Wang, Z. Wang, S. Wu, H. Liu, Z. Lu, Facile electrodeposition of 3D concentration-gradient Ni-Co hydroxide nanostructures on nickel foam as high performance electrodes for asymmetric supercapacitors, Nano Res. 8 (2015) 2744–2754, https://doi.org/10.1007/s12274-015-0781-3.

[40] R. Jia, C. Zhao, Z. Huang, X. Liu, D. Wang, Z. Hui, X. Xu, An in situ growth strategy of NiCo-MOF nanosheets with more activity sites for asymmetric supercapacitors, Ionics (2020), https://doi.org/10.1007/s11581-020-03727-x.

[41] S.C. Lee, S. Liu, P.A. Shinde, K.Y. Chung, S. Chan Jun, A systematic approach to achieve high energy density hybrid supercapacitors based on Ni–Co–Fe hydroxide, Electrochim. Acta 353 (2020), 136578, https://doi.org/10.1016/j.electacta.2020.136578.

[42] L. Jiang, Y. Sui, J. Qi, Y. Chang, Y. He, Q. Meng, F. Wei, Z. Sun, Y. Jin, Hierarchical Ni-Co layered double hydroxide nanosheets on functionalized 3D-RGO films for high energy density asymmetric supercapacitor, Appl. Surf. Sci. 426 (2017) 148–159, https://doi.org/10.1016/j.apsusc.2017.07.175.

[43] J. Cao, L. Li, Y. Xi, J. Li, X. Pan, D. Chen, W. Han, Core–shell structural PANI-derived carbon@Co–Ni LDH electrode for high-performance asymmetric supercapacitors, Sustain. Energy Fuels 2 (2018) 1350–1355, https://doi.org/10.1039/C8SE00123E.

[44] M. Li, R. Jijie, A. Barras, P. Roussel, S. Szunerits, R. Boukherroub, NiFe layered double hydroxide electrodeposited on Ni foam coated with reduced graphene oxide for high-performance supercapacitors, Electrochim. Acta 302 (2019) 1–9, https://doi.org/10.1016/j.electacta.2019.01.187.

[45] A.D. Jagadale, G. Guan, X. Li, X. Du, X. Ma, X. Hao, A. Abudula, Binder-free electrodes of CoAl layered double hydroxide on carbon fibers for all-solid-state flexible yarn supercapacitors, Energy Technol. 4 (2016) 997–1004, https://doi.org/10.1002/ente.201600018.

[46] G. Luo, K. Siong Teh, Y. Xia, Y. Luo, Z. Li, S. Wang, L. Zhao, Z. Jiang, A novel three-dimensional spiral CoNi LDHs on Au@ErGO wire for high performance fiber supercapacitor electrodes, Mater. Lett. 236 (2019) 728–731, https://doi.org/10.1016/j.matlet.2018.11.038.

[47] Q. Yang, Z. Li, R. Zhang, L. Zhou, M. Shao, M. Wei, Carbon modified transition metal oxides/hydroxides nanoarrays toward high-performance flexible all-solid-state supercapacitors, Nano Energy 41 (2017) 408–416, https://doi.org/10.1016/j.nanoen.2017.09.049.

[48] Y. Li, L. Wang, Y. Qu, B. Wang, J. Yu, D. Song, C. Duan, Y. Yang, Unique 3D bilayer nanostructure basic cobalt carbonate@NiCo–layered double hydroxide nanosheets on carbon cloth for supercapacitor electrode material, Ionics 26 (2020) 1397–1406, https://doi.org/10.1007/s11581-019-03310-z.

[49] S. Shahrokhian, S. Rahimi, R. Mohammadi, Nickel-cobalt layered double hydroxide ultrathin nanosheets coated on reduced graphene oxide nonosheets/nickel foam for high performance asymmetric supercapacitors, Int. J. Hydrogen Energy 43 (2018) 2256–2267, https://doi.org/10.1016/j.ijhydene.2017.12.019.

[50] X. Wang, T. Song, Buckypaper templating Ni–Co hydroxide nanosheets as free-standing electrodes for ultrathin and flexible supercapacitors, New J. Chem. 40 (2016) 8006–8011, https://doi.org/10.1039/C6NJ01470D.

[51] A. Adán-Más, R.G. Duarte, T.M. Silva, L. Guerlou-Demourgues, M.F.G. Montemor, Enhancement of the Ni-Co hydroxide response as energy storage material by electrochemically reduced graphene oxide, Electrochim. Acta 240 (2017) 323–340, https://doi.org/10.1016/j.electacta.2017.04.070.

[52] Y. Li, L. Shan, Y. Sui, J. Qi, F. Wei, Y. He, Q. Meng, Y. Ren, J. Liu, Ultrathin Ni–Co LDH nanosheets grown on carbon fiber cloth via electrodeposition for high-performance supercapacitors, J. Mater. Sci. Mater. Electron. 30 (2019) 13360–13371, https://doi.org/10.1007/s10854-019-01703-4.

[53] T. Nguyen, M. Boudard, M. João Carmezim, M. Fátima Montemor, NixCo1-x $(OH)_2$ nanosheets on carbon nanofoam paper as high areal capacity electrodes for hybrid supercapacitors, Energy 126 (2017) 208–216, https://doi.org/10.1016/j.energy.2017.03.024.

[54] A.M. Zardkhoshoui, S.S. Hosseiny Davarani, All-solid-state, flexible, ultrahigh performance supercapacitors based on the Ni-Al LDH-rGO electrodes, J. Alloys Compd. 750 (2018) 515–522, https://doi.org/10.1016/j.jallcom.2018.04.027.

[55] Y.J. Yang, W. Li, Hierarchical Ni–Co double hydroxide nanosheets on reduced graphene oxide self-assembled on Ni foam for high-energy hybrid supercapacitors, J. Alloys Compd. 776 (2019) 543–553, https://doi.org/10.1016/j.jallcom.2018.10.344.

[56] C. Xin, L. Ang, F. Musharavati, F. Jaber, L. Hui, E. Zalnezhad, S. Bae, K.S. Hui, K. N. Hui, Supercapacitor performance of nickel-cobalt sulfide nanotubes decorated using Ni Co-layered double hydroxide nanosheets grown in situ on Ni foam, Nanomaterials 10 (2020) 584, https://doi.org/10.3390/nano10030584.

[57] J. Xing, J. Du, X. Zhang, Y. Shao, T. Zhang, C. Xu, A Ni-P@NiCo LDH core–shell nanorod-decorated nickel foam with enhanced areal specific capacitance for high-performance supercapacitors, Dalton Trans. 46 (2017) 10064–10072, https://doi.org/10.1039/C7DT01910F.

[58] Y. Wang, S. Dong, X. Wu, M. Li, One-step electrodeposition of MnO_2@NiAl layered double hydroxide nanostructures on the nickel foam for high-performance supercapacitors, J. Electrochem. Soc. 164 (2016) H56, https://doi.org/10.1149/2.0861702jes.

[59] S. Wang, Z. Huang, R. Li, X. Zheng, F. Lu, T. He, Template-assisted synthesis of NiP@CoAl-LDH nanotube arrays with superior electrochemical performance for supercapacitors, Electrochim. Acta 204 (2016) 160–168, https://doi.org/10.1016/j.electacta.2016.04.051.

[60] P. Naveenkumar, G. Paruthimal Kalaignan, Fabrication of core-shell like hybrids of CuCo2S4@NiCo$(OH)_2$ nanosheets for supercapacitor applications, Compos. Part B Eng. 173 (2019), 106864, https://doi.org/10.1016/j.compositesb.2019.05.075.

[61] Y. Zhang, Z. Shi, L. Liu, Y. Gao, J. Liu, High conductive architecture: bimetal oxide with metallic properties @ bimetal hydroxide for high-performance pseudocapacitor, Electrochim. Acta 231 (2017) 487–494, https://doi.org/10.1016/j.electacta.2017.02.076.

[62] N. Zhao, H. Fan, M. Zhang, C. Wang, X. Ren, H. Peng, H. Li, X. Jiang, X. Cao, Preparation of partially-cladding NiCo-LDH/Mn_3O_4 composite by electrodeposition route and its excellent supercapacitor performance, J. Alloys Compd. 796 (2019) 111–119, https://doi.org/10.1016/j.jallcom.2019.05.023.

[63] Y. Liu, N. Fu, G. Zhang, M. Xu, W. Lu, L. Zhou, H. Huang, Design of Hierarchical Ni—Co@Ni—Co layered double hydroxide core–shell structured nanotube array for high-performance flexible all-solid-state battery-type supercapacitors, Adv. Funct. Mater. 27 (2017), 1605307, https://doi.org/10.1002/adfm.201605307.

[64] N. Karthik, T.N.J.I. Edison, R. Atchudan, D. Xiong, Y.R. Lee, Electro-synthesis of sulfur doped nickel cobalt layered double hydroxide for electrocatalytic hydrogen evolution reaction and supercapacitor applications, J. Electroanal. Chem. 833 (2019) 105–112, https://doi.org/10.1016/j.jelechem.2018.11.028.

[65] G. Liu, X.-Z. Song, S. Zhang, X. Chen, S. Liu, Y. Meng, Z. Tan, Hierarchical CuO@ZnCo–OH core-shell heterostructure on copper foam as three-dimensional binder-free electrodes for high performance asymmetric supercapacitors, J. Power Sources 465 (2020), 228239, https://doi.org/10.1016/j.jpowsour.2020.228239.

[66] V.T. Chebrolu, B. Balakrishnan, V. Raman, I. Cho, J.-S. Bak, K. Prabakar, H.-J. Kim, Co-electrodeposition of NiCu(OH)2@Ni-Cu-Se hierarchical nanoparticle structure for supercapacitor application with enhanced performance, Appl. Surf. Sci. 506 (2020), 145015, https://doi.org/10.1016/j.apsusc.2019.145015.

[67] Y. Chuminjak, P. Singjai, A. Tuantranont, C. Sriprachuabwong, A. Wisitsoraat, High-capacity charge storage electrodes based on nickel oxide and nickel–cobalt double hydroxide nanocomposites on 3D nickel foam prepared by sparking and electrodeposition, J. Alloys Compd. 841 (2020), 155793, https://doi.org/10.1016/j.jallcom.2020.155793.

[68] Y. Tang, B. Cheng, 3D self-supported hierarchical NiCo architectures with integrated capacitive performance and enhanced electronic conductivity for supercapacitors, Energy 112 (2016) 755–761, https://doi.org/10.1016/j.energy.2016.06.104.

[69] H. Li, F. Musharavati, E. Zalenezhad, X. Chen, K.N. Hui, K.S. Hui, Electrodeposited NiCo layered double hydroxides on titanium carbide as a binder-free electrode for supercapacitors, Electrochim. Acta 261 (2018) 178–187, https://doi.org/10.1016/j.electacta.2017.12.139.

[70] Y. Yan, B. Yu Xia, B. Zhao, X. Wang, A review on noble-metal-free bifunctional heterogeneous catalysts for overall electrochemical water splitting, J. Mater. Chem. A 4 (2016) 17587–17603, https://doi.org/10.1039/C6TA08075H.

[71] D. Yang, L. Zhang, X. Yan, X. Yao, Recent progress in oxygen electrocatalysts for zinc–air batteries, Small Methods 1 (2017), 1700209, https://doi.org/10.1002/smtd.201700209.

[72] M. Prabu, P. Ramakrishnan, S. Shanmugam, $CoMn_2O_4$ nanoparticles anchored on nitrogen-doped graphene nanosheets as bifunctional electrocatalyst for rechargeable zinc–air battery, Electrochem. Commun. 41 (2014) 59–63, https://doi.org/10.1016/j.elecom.2014.01.027.

[73] J.-S. Lee, G.S. Park, H.I. Lee, S.T. Kim, R. Cao, M. Liu, J. Cho, Ketjenblack carbon supported amorphous manganese oxides nanowires as highly efficient electrocatalyst for oxygen reduction reaction in alkaline solutions, Nano Lett. 11 (2011) 5362–5366, https://doi.org/10.1021/nl2029078.

[74] S. Srinivasan, H. Wroblowa, J.O.M. Bockris, Electrocatalysis, in: D.D. Eley, H. Pines, P.B. Weisz (Eds.), Advances in Catalysis, Academic Press, 1967, pp. 351–418, https://doi.org/10.1016/S0360-0564(08)60690-2.

[75] P. Babar, A. Lokhande, H.H. Shin, B. Pawar, M.G. Gang, S. Pawar, J.H. Kim, Cobalt Iron hydroxide as a precious metal-free bifunctional electrocatalyst for efficient overall water splitting, Small 14 (2018), 1702568, https://doi.org/10.1002/smll.201702568.

[76] W. Liu, H. Liu, L. Dang, H. Zhang, X. Wu, B. Yang, Z. Li, X. Zhang, L. Lei, S. Jin, Amorphous cobalt–iron hydroxide nanosheet electrocatalyst for efficient electrochemical and photo-electrochemical oxygen evolution, Adv. Funct. Mater. 27 (2017), 1603904, https://doi.org/10.1002/adfm.201603904.

[77] Y. Pei, Y. Ge, H. Chu, W. Smith, P. Dong, P.M. Ajayan, M. Ye, J. Shen, Controlled synthesis of 3D porous structured cobalt-iron based nanosheets by electrodeposition as asymmetric electrodes for ultra-efficient water splitting, Appl. Catal. B Environ. 244 (2019) 583–593, https://doi.org/10.1016/j.apcatb.2018.11.091.

[78] A.M.P. Sakita, R.D. Noce, E. Vallés, A.V. Benedetti, Pulse electrodeposition of CoFe thin films covered with layered double hydroxides as a fast route to prepare enhanced catalysts for oxygen evolution reaction, Appl. Surf. Sci. 434 (2018) 1153–1160, https://doi.org/10.1016/j.apsusc.2017.11.042.

[79] S. Yoon, J.-Y. Yun, J.-H. Lim, B. Yoo, Enhanced electrocatalytic properties of electrodeposited amorphous cobalt-nickel hydroxide nanosheets on nickel foam by the formation of nickel nanocones for the oxygen evolution reaction, J. Alloys Compd. 693 (2017) 964–969, https://doi.org/10.1016/j.jallcom.2016.09.247.

[80] X. Bo, Y. Li, X. Chen, C. Zhao, High valence chromium regulated cobalt-iron-hydroxide for enhanced water oxidation, J. Power Sources 402 (2018) 381–387, https://doi.org/10.1016/j.jpowsour.2018.09.063.

[81] F. Yan, D. Guo, J. Kang, L. Liu, C. Zhu, P. Gao, X. Zhang, Y. Chen, Fast fabrication of ultrathin CoMn LDH nanoarray as flexible electrode for water oxidation, Electrochim. Acta 283 (2018) 755–763, https://doi.org/10.1016/j.electacta.2018.06.202.

[82] Y. Sun, C. Liu, L. Zhang, P. Wan, S. Zhuang, Y. Tang, Y. Chen, J. Pan, Ultrafast electrodeposition of Ni−Fe hydroxide nanosheets on nickel foam as oxygen evolution anode for energy-saving electrolysis of Na_2 CO_3/$NaHCO_3$, ChemElectroChem 4 (2017) 1044–1050, https://doi.org/10.1002/celc.201600713.

[83] A.S. Batchellor, S.W. Boettcher, Pulse-electrodeposited Ni–Fe (Oxy)hydroxide oxygen evolution electrocatalysts with high geometric and intrinsic activities at large mass loadings, ACS Catal. 5 (2015) 6680–6689, https://doi.org/10.1021/acscatal.5b01551.

[84] H. Yang, S. Luo, Y. Bao, Y. Luo, J. Jin, J. Ma, In situ growth of ultrathin Ni–Fe LDH nanosheets for high performance oxygen evolution reaction, Inorg. Chem. Front. 4 (2017) 1173–1181, https://doi.org/10.1039/C7QI00167C.

[85] J. Shen, M. Wang, L. Zhao, J. Jiang, H. Liu, J. Liu, Self-supported stainless steel nanocone array coated with a layer of Ni–Fe oxides/(Oxy)hydroxides as a highly active and robust electrode for water oxidation, ACS Appl. Mater. Interfaces 10 (2018) 8786–8796, https://doi.org/10.1021/acsami.8b00498.

[86] H. Wei, Studies on the effect of the substrate on the electrocatalytic performance of electrodeposited NiFe hydroxides for oxygen evolution reaction, Int. J. Electrochem. Sci. (2019) 4173–4184, https://doi.org/10.20964/2019.05.45. School of Materials Science and Engineering, Tianjin University, Tianjin 300072, China.

[87] P. Babar, A. Lokhande, V. Karade, B. Pawar, M.G. Gang, S. Pawar, J.H. Kim, Bifunctional 2D electrocatalysts of transition metal hydroxide nanosheet arrays for water splitting and urea electrolysis, ACS Sustain. Chem. Eng. 7 (2019) 10035–10043, https://doi.org/10.1021/acssuschemeng.9b01260.

[88] X. Bo, Y. Li, R.K. Hocking, C. Zhao, NiFeCr hydroxide holey nanosheet as advanced electrocatalyst for water oxidation, ACS Appl. Mater. Interfaces 9 (2017) 41239–41245, https://doi.org/10.1021/acsami.7b12629.

[89] Y. Li, L. Zhang, X. Xiang, D. Yan, F. Li, Engineering of ZnCo-layered double hydroxide nanowalls toward high-efficiency electrochemical water oxidation, J. Mater. Chem. A 2 (2014) 13250–13258, https://doi.org/10.1039/C4TA01275E.

[90] H. Li, L. Zhang, S. Wang, J. Yu, Accelerated oxygen evolution kinetics on NiFeAl-layered double hydroxide electrocatalysts with defect sites prepared by electrodeposition, Int. J. Hydrogen Energy 44 (2019) 28556–28565, https://doi.org/10.1016/j.ijhydene.2019.09.155.

[91] L. Hu, M. Li, X. Wei, H. Wang, Y. Wu, J. Wen, W. Gu, C. Zhu, Modulating interfacial electronic structure of CoNi LDH nanosheets with Ti_3C_2Tx MXene for enhancing water oxidation catalysis, Chem. Eng. J. 398 (2020), 125605, https://doi.org/10.1016/j.cej.2020.125605.

[92] X. Yu, M. Zhang, W. Yuan, G. Shi, A high-performance three-dimensional Ni–Fe layered double hydroxide/graphene electrode for water oxidation, J. Mater. Chem. A 3 (2015) 6921–6928, https://doi.org/10.1039/C5TA01034A.

[93] X. Ma, X. Li, A.D. Jagadale, X. Hao, A. Abudula, G. Guan, Fabrication of Cu$(OH)_2$@NiFe-layered double hydroxide catalyst array for electrochemical water splitting, Int. J. Hydrogen Energy 41 (2016) 14553–14561, https://doi.org/10.1016/j.ijhydene.2016.05.174.

[94] P. Wang, Y. Lin, L. Wan, B. Wang, Construction of a janus MnO_2-NiFe electrode via selective electrodeposition strategy as a high-performance bifunctional electrocatalyst for rechargeable zinc–air batteries, ACS Appl. Mater. Interfaces 11 (2019) 37701–37707, https://doi.org/10.1021/acsami.9b12232.

[95] H.S. Jadhav, A. Roy, B.Z. Desalegan, J. Gil Seo, An advanced and highly efficient Ce assisted NiFe-LDH electrocatalyst for overall water splitting, Sustain. Energy Fuels 4 (2020) 312–323, https://doi.org/10.1039/C9SE00700H.

[96] P. Wang, L. Wan, Y. Lin, B. Wang, NiFe hydroxide supported on hierarchically porous nickel mesh as a high-performance bifunctional electrocatalyst for water splitting at large current density, ChemSusChem 12 (2019) 4038–4045, https://doi.org/10.1002/cssc.201901439.

[97] X. Yu, Y. Kang, S. Wang, K.S. Hui, K.N. Hui, H. Zhao, J. Li, B. Li, J. Xu, L. Chen, H. Shao, Integrating PtNi nanoparticles on NiFe layered double hydroxide nanosheets as a bifunctional catalyst for hybrid sodium–air batteries, J. Mater. Chem. A 8 (2020) 16355–16365, https://doi.org/10.1039/D0TA04602G.

[98] X. Han, N. Suo, C. Chen, Z. Lin, Z. Dou, X. He, L. Cui, Graphene oxide guiding the constructing of nickel-iron layered double hydroxides arrays as a desirable bifunctional electrocatalyst for HER and OER, Int. J. Hydrogen Energy 44 (2019) 29876–29888, https://doi.org/10.1016/j.ijhydene.2019.09.116.

[99] H. Wang, L. Gao, Recent developments in electrochemical hydrogen evolution reaction, Curr. Opin. Electrochem. 7 (2018) 7–14, https://doi.org/10.1016/j.coelec.2017.10.010.

[100] M. Yao, B. Wang, N. Wang, S. Komarneni, Y. Chen, J. Wang, X. Niu, W. Hu, Self-supported composite of (Ni,Co)3C mesoporous nanosheets/N-doped carbon as a flexible electrocatalyst for pH-universal hydrogen evolution, ACS Sustain. Chem. Eng. 8 (2020) 5287–5295, https://doi.org/10.1021/acssuschemeng.0c00268.

[101] M. Shao, Q. Chang, J.-P. Dodelet, R. Chenitz, Recent advances in electrocatalysts for oxygen reduction reaction, Chem. Rev. 116 (2016) 3594–3657, https://doi.org/10.1021/acs.chemrev.5b00462.

[102] E. Mustafa, A. Tahira, R.E. Adam, Z.H. Ibupoto, S. Elhag, M. Willander, O. Nur, Efficient Ni–Fe layered double hydroxides/ZnO nanostructures for photochemical water splitting, J. Solid State Chem. 273 (2019) 186–191, https://doi.org/10.1016/j.jssc.2019.03.004.
[103] L. Sun, J. Sun, X. Yang, S. Bai, Y. Feng, R. Luo, D. Li, A. Chen, An integrating photoanode consisting of BiVO4, rGO and LDH for photoelectrochemical water splitting, Dalton Trans. 48 (2019) 16091–16098, https://doi.org/10.1039/C9DT01819K.
[104] Y. Zhu, X. Zhao, J. Li, H. Zhang, S. Chen, W. Han, D. Yang, Surface modification of hematite photoanode by NiFe layered double hydroxide for boosting photoelectrocatalytic water oxidation, J. Alloys Compd. 764 (2018) 341–346, https://doi.org/10.1016/j.jallcom.2018.06.064.
[105] R. Zhang, M. Shao, S. Xu, F. Ning, L. Zhou, M. Wei, Photo-assisted synthesis of zinc-iron layered double hydroxides/TiO_2 nanoarrays toward highly-efficient photoelectrochemical water splitting, Nano Energy 33 (2017) 21–28, https://doi.org/10.1016/j.nanoen.2017.01.020.
[106] D. Xu, Y. Rui, Y. Li, Q. Zhang, H. Wang, Zn-Co layered double hydroxide modified hematite photoanode for enhanced photoelectrochemical water splitting, Appl. Surf. Sci. 358 (2015) 436–442, https://doi.org/10.1016/j.apsusc.2015.08.160.
[107] Y. Wang, D. Zhang, W. Peng, L. Liu, M. Li, Electrocatalytic oxidation of methanol at Ni–Al layered double hydroxide film modified electrode in alkaline medium, Electrochim. Acta 56 (2011) 5754–5758, https://doi.org/10.1016/j.electacta.2011.04.049.
[108] M.K. Kumar, K.C. Swaathini, N.S. Jha, S.K. Jha, Facile in situ electrosynthesis and high electrocatalytic performance of interconnected layered double hydroxides/graphene hybrids for dopamine oxidation: a comparative study, Electroanalysis 31 (2019) 485–495, https://doi.org/10.1002/elan.201800542.
[109] M. Heidari, A. Ghaffarinejad, Electrochemical sensor for L-cysteine by using a cobalt(II)/aluminum(III) layered double hydroxide as a nanocatalyst, Microchim. Acta 186 (2019) 365, https://doi.org/10.1007/s00604-019-3462-1.
[110] L. Wu, J. Li, H.-M. Zhang, One step fabrication of Au nanoparticles-Ni-Al layered double hydroxide composite film for the determination of L-cysteine, Electroanalysis 27 (2015) 1195–1201, https://doi.org/10.1002/elan.201400624.
[111] I. Carpani, L. Guadagnini, D. Tonelli, Lactate biosensor based on hydrotalcite-like compounds: performances and application to serum samples, Electroanalysis 21 (2009) 2401–2409, https://doi.org/10.1002/elan.200900118.
[112] H. Liang, X. Miao, J. Gong, One-step fabrication of layered double hydroxides/graphene hybrid as solid-phase extraction for stripping voltammetric detection of methyl parathion, Electrochem. Commun. 20 (2012) 149–152, https://doi.org/10.1016/j.elecom.2012.04.010.
[113] J. Ju, J. Bai, X. Bo, L. Guo, Non-enzymatic acetylcholine sensor based on Ni–Al layered double hydroxides/ordered mesoporous carbon, Electrochim. Acta 78 (2012) 569–575, https://doi.org/10.1016/j.electacta.2012.06.051.
[114] N. Shishegari, A. Sabahi, F. Manteghi, A. Ghaffarinejad, Z. Tehrani, Non-enzymatic sensor based on nitrogen-doped graphene modified with Pd nanoparticles and NiAl layered double hydroxide for glucose determination in blood, J. Electroanal. Chem. 871 (2020), 114285, https://doi.org/10.1016/j.jelechem.2020.114285.
[115] A. Mignani, C. Corticelli, D. Tonelli, E. Scavetta, A new pH sensor based on a glassy carbon electrode coated with a Co/Al layered double hydroxide, Electroanalysis 23 (2011) 1745–1751, https://doi.org/10.1002/elan.201100058.
[116] X. Qiao, M. Wei, D. Tian, F. Xia, P. Chen, C. Zhou, One-step electrosynthesis of cadmium/aluminum layered double hydroxides composite as electrochemical probe for voltammetric detection of anthracene, J. Electroanal. Chem. 808 (2018) 35–40, https://doi.org/10.1016/j.jelechem.2017.11.063.
[117] Q.-Q. He, M.-J. Zhou, J.-M. Hu, Electrodeposited Zn-Al layered double hydroxide films for corrosion protection of aluminum alloys, Electrochim. Acta 355 (2020), 136796, https://doi.org/10.1016/j.electacta.2020.136796.
[118] X. Yin, P. Mu, Q. Wang, J. Li, Superhydrophobic ZIF-8-based dual-layer coating for enhanced corrosion protection of Mg alloy, ACS Appl. Mater. Interfaces 12 (2020) 35453–35463, https://doi.org/10.1021/acsami.0c09497.
[119] Y. Yang, X. Du, A. Abudula, Z. Zhang, X. Ma, K. Tang, X. Hao, G. Guan, Highly efficient defluoridation using a porous MWCNT@NiMn-LDH composites based on ion transport of EDL coupled with ligand exchange mechanism, Sep. Purif. Technol. 223 (2019) 154–161, https://doi.org/10.1016/j.seppur.2019.04.052.
[120] J. Wang, F. Gao, X. Du, X. Ma, X. Hao, W. Ma, K. Wang, G. Guan, A. Abudula, A high-performance electroactive PPy/rGO/NiCo-LDH hybrid film for removal of dilute dodecyl sulfonate ions, Electrochim. Acta 331 (2020), 135288, https://doi.org/10.1016/j.electacta.2019.135288.
[121] M. Shamsayei, Y. Yamini, H. Asiabi, M.M. Khataei, Electrodeposition of layered double hydroxide intercalated with 2,3-dimercaptopropane sulfonate on carbon cloth and application for effective uptake of heavy metals, Appl. Clay Sci. 196 (2020), 105747, https://doi.org/10.1016/j.clay.2020.105747.